Geomorphology 361 (2020) 107192

Contents lists available at ScienceDirect

Geomorphology

journal homepage: www.elsevier.com/locate/geomorph

The glacial landsystem of Fjallsjökull, Iceland: Spatial and temporal evolution of process-form regimes at an active temperate glacier

Benjamin M.P. Chandler [a,b,*], David J.A. Evans [c], Samuel J.P. Chandler [a], Marek W. Ewertowski [d], Harold Lovell [a], David H. Roberts [c], Martin Schaefer [a], Aleksandra M. Tomczyk [d]

[a] School of the Environment, Geography and Geosciences, University of Portsmouth, Portsmouth, UK
[b] Department of Physical Geography, Stockholm University, Stockholm, Sweden
[c] Department of Geography, Durham University, Durham, UK
[d] Faculty of Geographical and Geological Sciences, Adam Mickiewicz University, Poznań, Poland

ARTICLE INFO

Article history:
Received 29 January 2020
Received in revised form 31 March 2020
Accepted 31 March 2020
Available online 01 April 2020

Keywords:
Active temperate glacial landsystems
Glacial landscape change
Glacial geomorphological mapping
UAV surveying
Fjallsjökull
Iceland

ABSTRACT

This study assesses the spatial and temporal evolution of the glacial landsystem signature at Fjallsjökull, southeast Iceland, using (a) mapping of the glacial geomorphology and surficial geology and (b) repeat uncrewed aerial vehicle (UAV) surveys. A small-scale (1: 15,000 scale) landsystem map has been compiled using LiDAR data (2011−2012) and historical aerial photographs (1945–1998), along with a large-scale (1: 2000 scale) map based on UAV imagery from May 2019. From our mapping and UAV surveys, we identify sediment-landform assemblages that are typical of active temperate glacial landsystems, including recessional push/squeeze moraines and intervening flutings, overridden moraine arcs, proglacial outwash (sandur) fans and linear/ribbon sandar. We recognize three landform zones that are defined by changes in moraine morphology and the nature of proglacial outwash deposition: (1) the outer foreland is characterized by proglacial outwash fans, overridden moraine arcs and broadly linear recessional moraines; (2) the middle foreland contains sawtooth moraines and linear sandar; and (3) the innermost zone comprises extremely sawtooth and hairpin moraines as well as associated crevasse-squeeze ridge limbs. This landform zonation reflects spatio-temporal changes in moraine-forming processes and outwash deposition as determined by changes in snout morphology and proglacial drainage characteristics. Within this general tripartite zonation, we also identify localized (azonal/intrazonal) sediment-landform assemblages that are not typically found at active temperate glaciers, including ice-cored/hummocky terrain and localized kame and kettle topography. Repeat UAV surveying in 2016–2019 has allowed us to capture and quantify recent intrazonal landsystem change at the southern glacier margin. We identify a switch from moraine formation to the development of ice-cored terrain and an ice-cored esker complex in association with the uncovering of a depositional overdeepening. Our study demonstrates the important role that variations in local boundary conditions (e.g. topography) can play in the process-form response of individual active temperate outlet glaciers, contributing to the expanding database on modern glacial landsystems.

1. Introduction

Assessing modern glacial landsystem signatures and their spatial and temporal evolution is important for developing modern, process-based analogues that can be applied to ancient deglaciated terrain (Evans, 2003a). In particular, landsystems research in modern glacial environments enables process-form regimes to be linked to specific glaciological, environmental and/or topographic conditions (e.g. Evans and Twigg, 2002; Bennett and Evans, 2012; Schomacker et al., 2014; Evans et al., 2016a, 2017a, 2019a; Ewertowski et al., 2019a). Such studies have allowed a large database of modern process-form analogues to be developed, and these landsystem models enable comparable sediment-landform assemblages in ancient glacial landscapes to be used as glaciodynamic and palaeoclimatic indicators (e.g. Evans et al., 2014, 2020; Darvill et al., 2017; Sutherland et al., 2019). More broadly, the development of modern glacial landsystem models and assessments of spatially-variable landsystem signatures are highly relevant to applied disciplines (e.g. civil engineering, the aggregate industry) in which understanding the nature of subsurface sediments in glaciated terrain is important (cf. Griffiths and Martin, 2017).

Icelandic glaciers have been a particular focus of modern glacial landsystems research (Krüger, 1994; Evans, 2003b, Evans, 2005; Ingólfsson et al., 2016), especially the outlets of the Öræfajökull and Vatnajökull ice-caps in southeast Iceland. Post-Little Ice Age (LIA)

* Corresponding author at: Department of Physical Geography, Stockholm University, 106 91 Stockholm, Sweden.
E-mail address: benjamin.chandler@natgeo.su.se (B.M.P. Chandler).

https://doi.org/10.1016/j.geomorph.2020.107192

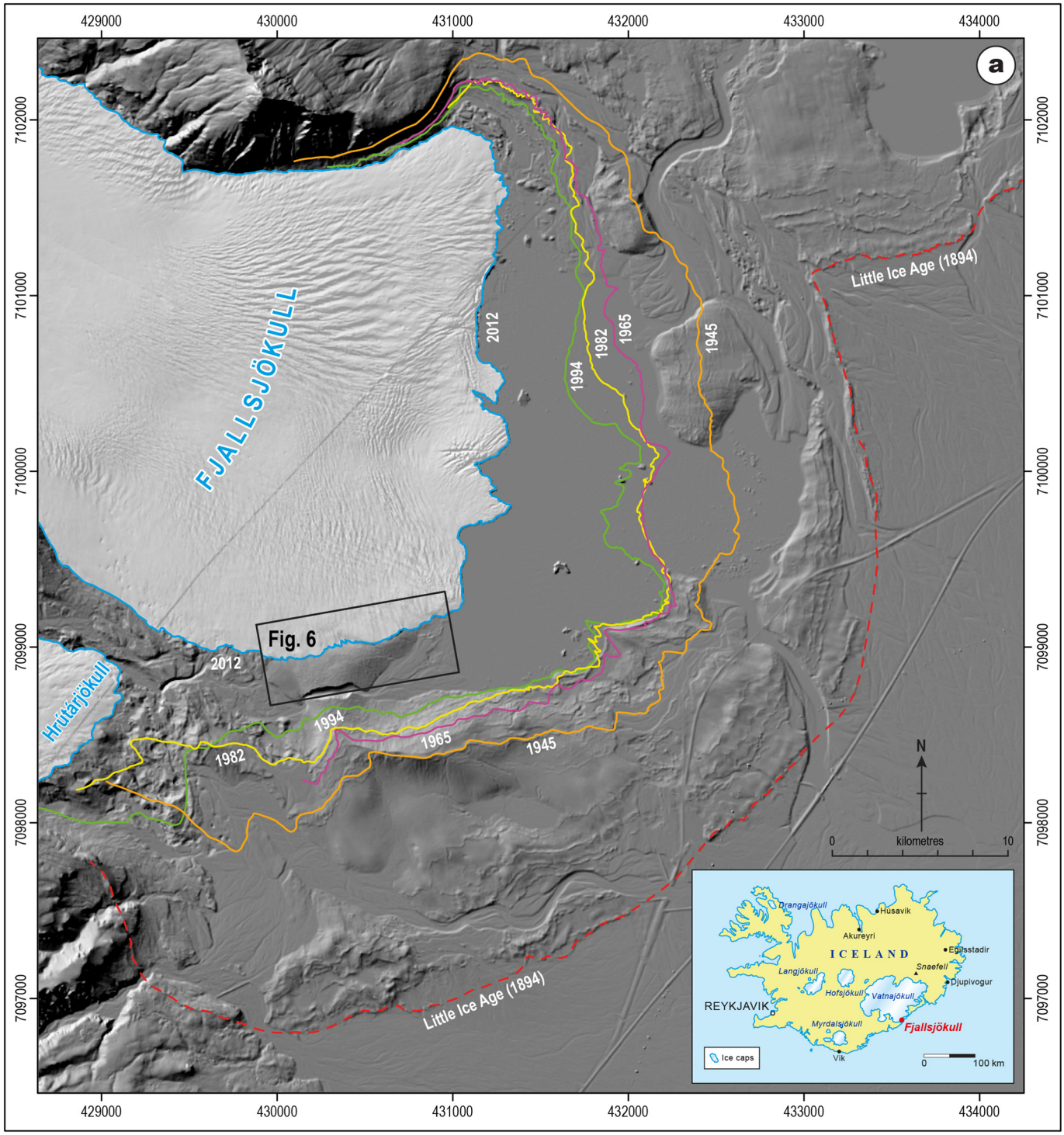

Fig. 1. (a) Location and overview of the Fjallsjökull foreland, southeast Iceland. The primary study area and location of our small-scale landsystem map (Fig. 6; Supplementary Material 2) are shown by the black frame. Selected former positions of the glacier margin are indicated, based on aerial photographs acquired from Landmælingar Íslands. The background hillshade relief model is based on LiDAR point-cloud data provided by the Icelandic Meteorological Office. The historical Little Ice Age date is based on archival data, as reported in Thórarinsson (1943). (b) Field photograph of Fjallsjökull and the proglacial lake, Fjallsárlón, in May 2019. The outlet glacier descends from the Öræfi caldera between Ærfjall (left) and Breiðmerkurfjall (right).

recession of those outlet glaciers is well documented both in historical archives and aerial imagery (e.g. Thórarinsson, 1943; Hannesdóttir et al., 2014, 2015), and this has facilitated the linkage of short-timescale glacial process-form regimes to climate trends at high (up to seasonal) resolution (e.g. Boulton, 1986; Evans and Twigg, 2002; Bradwell et al., 2013; Chandler et al., 2016a, 2016b, 2016c; Evans et al., 2016a, 2017a, 2017b, 2019a). The ice-cap outlets in southeast Iceland are predominantly active temperate glaciers, and their forelands are characterized by the diagnostic landsystem signature of recessional push/squeeze moraine sequences. In these settings, moraines are constructed by the emplacement of submarginally deforming till wedges, typically on an annual or seasonal timescale (Price, 1969, 1970; Boulton, 1986; Krüger, 1995; Evans and Twigg, 2002; Chandler et al., 2016a; Evans et al., 2018a).

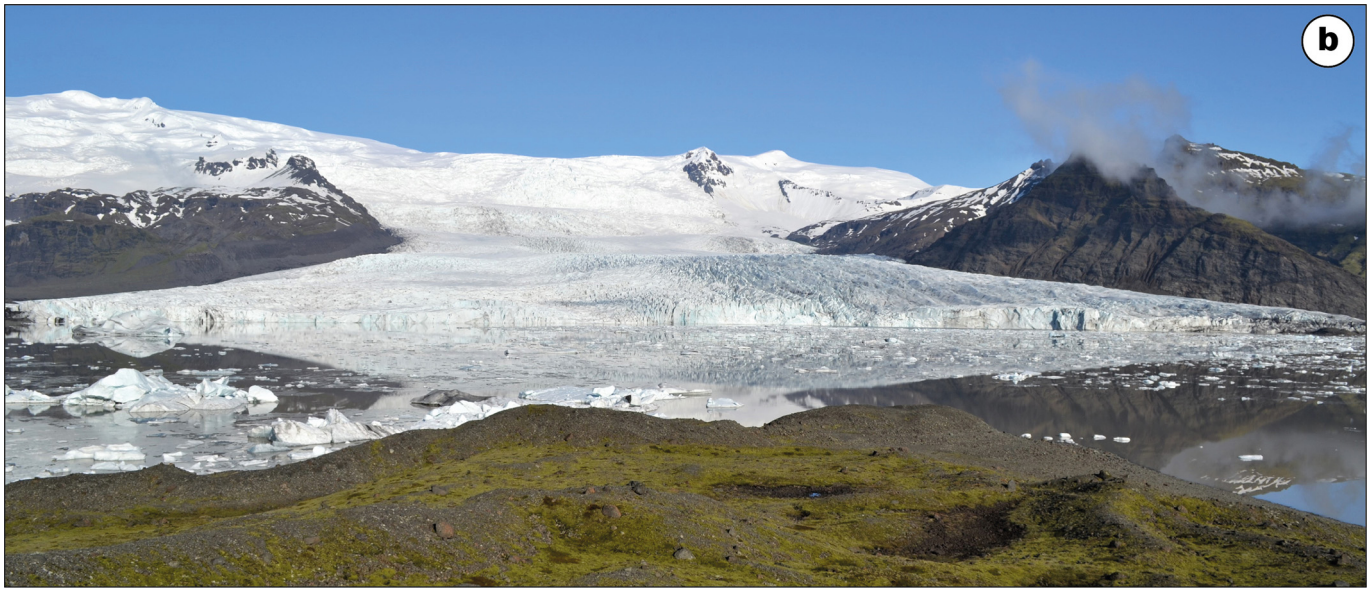

Fig. 1 (*continued*).

Within the overall active temperate process-form regimes, local overprinting and/or switching of landsystem signatures are particularly important. Such variations demonstrate the potential for locally diverse process-form responses of individual temperate glaciers to rapid climate change. Except for intermittent surge activity documented at Skeiðarárjökull and Breiðamerkurjökull (Boulton et al., 2001; Russell et al., 2001; Evans and Twigg, 2002; Björnsson et al., 2003; Waller et al., 2008, 2018), localized changes to glacial landsystem signatures (azonal and intrazonal changes; sensu Evans, 2013) are triggered by two factors: (i) climatically-driven glaciological changes; and/or (ii) topographically-controlled changes to the morphology and structural architecture of thinning glacier snouts. In recent decades, active temperate outlet glaciers in Iceland have exhibited a spatio-temporal change in their landsystem signatures, involving a switch from active temperate conditions and annual push/squeeze moraine formation to downwasting and calving in expanding proglacial lakes (e.g. Bennett et al., 2010; Bennett and Evans, 2012; Bradwell et al., 2013; Phillips et al., 2014; Evans and Orton, 2015; Everest et al., 2017). This switch is partly the result of accelerated climate warming since the late 20th century, but also reflects topographically-controlled changes in drainage conditions (e.g. Evans et al., 2016a, 2017a). Glacier snout recession into substantial overdeepenings (cf. Magnússon et al., 2012) or down the ice-contact slopes of sandur fans (outwash heads; sensu Kirkbride, 2000) has led to switches from unconfined, well-drained areas to constrained, relatively poorly-drained settings. Conversely, changing environmental conditions and glacier retreat down an adverse, poorly-drained slope has been recognized as the catalyst for the construction of multiple moraines per year at the southern margin of Skálafellsjökull (Chandler et al., 2016a). These observations of diversity in process-form responses highlight the need for continued monitoring of individual temperate glaciers to assess the impact of ongoing climate change.

In this study, we focus on the evolution of the glacial landsystem signature at Fjallsjökull, an outlet of Öræfajökull (Fig. 1), during recession of the snout from its Little Ice Age (LIA) maximum. Present glaciological and boundary conditions at the glacier snout are spatially diverse: the lake-terminating eastern margin is characterized by calving and rapid retreat (Dell et al., 2019), while the land-terminating southern margin is actively retreating down the adverse slope of a depositional overdeepening. Thus, Fjallsjökull represents a prime location for assessing localized spatially and temporally diverse process-form responses to changing climatic, glaciological and topographic conditions. This paper therefore has three aims: (i) to establish the spatial and temporal variations in the process-form response of Fjallsjökull since the LIA through glacial landsystem mapping; (ii) to quantify recent landscape changes at the glacier snout using repeat uncrewed aerial vehicle (UAV) surveying; and (iii) to link spatio-temporal changes in the landsystem signature to varying climatic, glaciological and topographic conditions at the glacier snout. This will provide a modern landsystem analogue for former active temperate glaciers that receded into depositional overdeepenings.

2. Study area

2.1. Glaciological setting

Fjallsjökull (64°01′N, 16°25′W) is a piedmont outlet lobe of Öræfajökull, situated in the southern part of Vatnajökull, southeast Iceland (Figs. 1 and 2). The outlet glacier and its neighbour, Hrútárjökull, are fed by ice flowing out eastwards from the Öræfi caldera. Fjallsjökull descends rapidly from its high-elevation ice divide at 2030 m a.s.l. over a series of bedrock steps to form an icefall between Ærfjall and Breiðmerkurfjall (Fig. 2b). The outlet lobe flows out onto a low elevation foreland, descending to near sea level (mean ~30 m a.s.l.). Fjallsjökull was formerly coalescent with the neighbouring Hrútárjökull and was historically also referred to as Hrútárjökull, before later being named Fjallsjökull (cf. Thórarinsson, 1943; Sigurðsson and Williams, 2008).

At its LIA maximum, the outlet splayed out to form a piedmont lobe that was coalescent with Breiðamerkurjökull (to the northeast) (Fig. 2; Thórarinsson, 1943; Evans and Twigg, 2002; Evans et al., 2009, 2019b). A maximum lichenometric age of 1727 CE was proposed by Bradwell (2004) for the outermost Fjallsjökull moraines, whereas Evans et al.

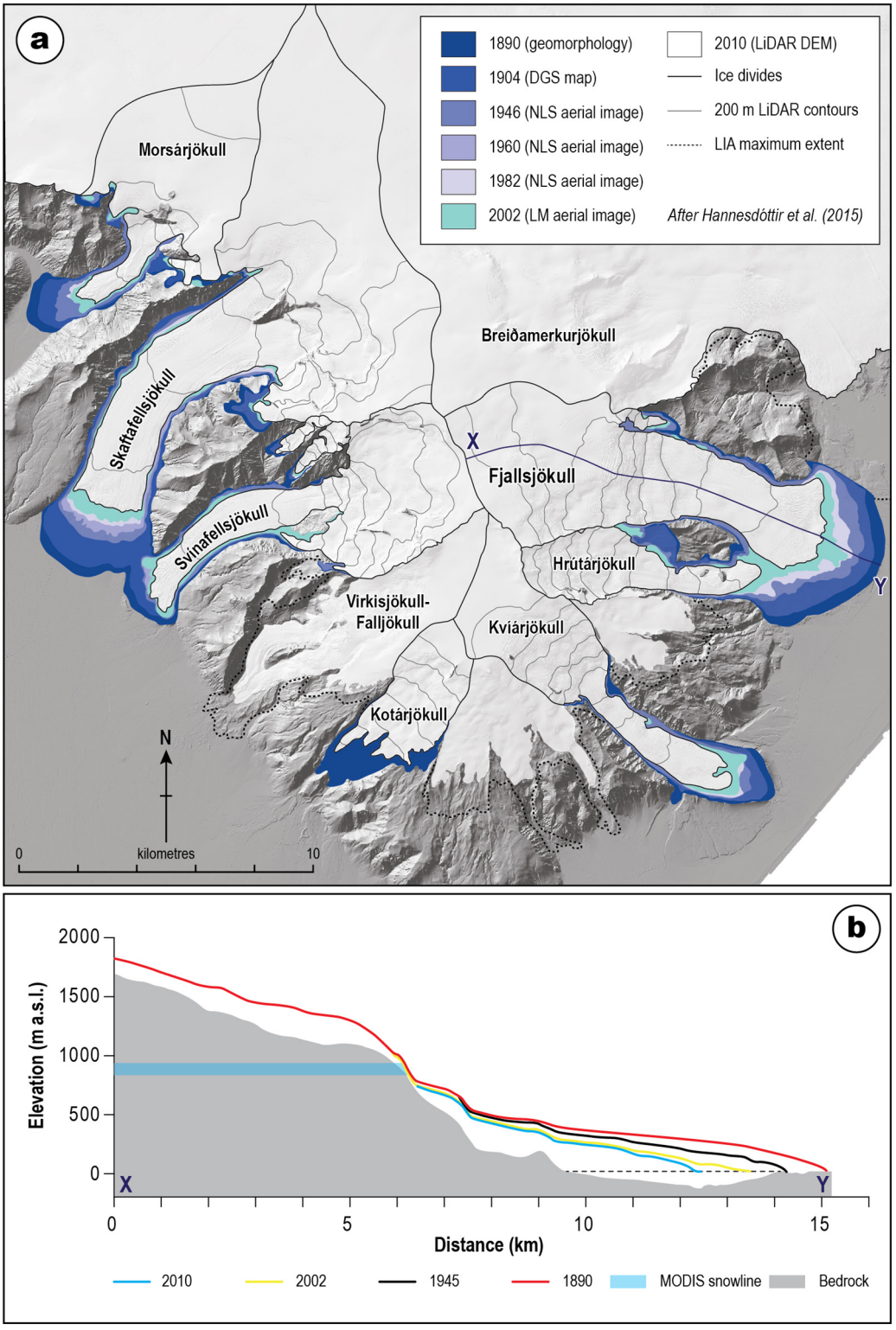

Fig. 2. (a) Map showing changes in glacier extent in the Öræfajökull region between 1890 and 2010 (after Hannesdóttir et al., 2015). The longitudinal profile X–Y is shown in (b). The ice extent in 1904 is uncertain in the mountains around Morsárjökull and Skaftafellsjökull due to distorted topography on the old map. The black dotted line indicates sea level and the location of an overdeepening (below the black dotted line). DGS: Danish General Staff; NLS: National Land Survey of Iceland; LM: Loftmyndir ehf. The 1890 glacier extent is from Hannesdóttir et al. (2014).

(2019b) derived an age of 1890 CE for the outermost Breiðamerkurjökull moraines. The latter lichenometric age is more consistent with historical archives that suggest Fjallsjökull reached its LIA maximum in 1870 CE before re-advancing to approximately the same position in 1894 CE (cf. Thórarinsson, 1943). Between the LIA and 2010, westwards retreat (~2.2 km) and thinning (mean ~28 m) of Fjallsjökull resulted in a 23% reduction in area and a 35% reduction in volume (Table 1; Hannesdóttir et al., 2015).

Regular ice-front measurements have been conducted at Fjallsjökull since the 1930s and compiled by the Icelandic Glaciological Society (Fig.

Table 1
Glaciological characteristics of Fjallsjökull in ~1890 (the LIA maximum) and 2010, based on the most recent assessment by Hannesdóttir et al. (2015).

Glaciological variable	~1890	2010	~1890–2010 change
Length (km)	15.1	12.9	−2.2 (−15%)
Average thickness (m)	185	157	−28 (−15%)
Area (km^2)	57.7 ± 0.8	44.6 ± 0.1	−13.1 ± 0.9 (−23%)
Volume (km^3)	10.7 ± 0.9	7.0 ± 0.02	−3.7 ± 1.0 (−35%)
ELA (m a.s.l.)	–	915 ± 45	–

3; e.g. Eyþórsson, 1935, 1963; Sigurðsson et al., 2007). Measurements at the land-terminating southern margin record rapid ice-margin retreat between 1935 and 1941 (~90 m a^{-1}), before more gradual retreat until the 1960s (1942–1959: ~9 m a^{-1}). A brief phase of rapid retreat followed between 1960 and 1963 (~46 m a^{-1}). Short-lived advances then occurred in the 1960s (1964–1966: ~21 m a^{-1}), 1970s (1974–1976: ~26 m a^{-1}), 1980s (1982–1983: ~16 m a^{-1}), and 1990s (1995–1996: ~19 m a^{-1}). From the 1990s until 2014, Fjallsjökull experienced sustained retreat at its southern margin (~35 m a^{-1}).

The westwards retreat of Fjallsjökull from its LIA limit during the 20th and 21st centuries has revealed a substantial overdeepening, which attains a maximum depth of 210 m and has a volume of 0.65 km^3 (Magnússon et al., 2012). The emergence of the overdeepening has led to development of a large proglacial lake (Fjallsárlón), into which the eastern Fjallsjökull margin terminates (Fig. 1b). Recent research has shown that the subglacial topography and continued expansion of the proglacial lake are important controls on ice flow and calving dynamics, with an increasingly spatially complex ice flow regime having developed over the past ~20 years (Dell et al., 2019). This ice flow regime is characterized by localized corridors of relatively high glacier surface velocities that have propagated towards the calving front.

2.2. Climatic setting

The Öræfi region experiences a relatively mild maritime climate with a low mean annual temperature range (~8–15 °C) and ~150 rain/snow days per year (Bradwell et al., 2013). Between 1884 and 2018, mean annual temperatures were between 2.5 and 6.4 °C at Fagurhólsmyrí (station 745; 63°53′N, 16°39′W; 46 m a.s.l.), the closest long-term weather station to Fjallsjökull (~20 km to the southwest). Mean summer temperatures ranged between 7.2 and 11.0 °C (average ~9.5 °C) for the entire record, but summer daily maxima of 20 °C are not uncommon in the Öræfi area. Mean temperatures during the winter ranged between −2.2 °C and 3.2 °C (average ~0.7 °C), with daily minima below −5 °C relatively rare. The eastern side of the Öræfi mountains, where Fjallsjökull is located, experiences relatively high annual precipitation totals that can locally exceed 7000 mm a^{-1} on the summit plateau (Guðmundsson, 2000). Measurements at Kvísker (station 740; 63°58′N, 16°26′W; ~30 m a.s.l.), situated ~6 km to the southwest of Fjallsjökull, indicate annual precipitation totals ranged between ~2560 and 4630 mm a^{-1} (average ~3510 mm a^{-1}; 1962–2011). Snow lies on the low ground (<200 m) of the Öræfi region for only 3–4 weeks per year on average (Bradwell et al., 2013), while permanently frozen ground is absent; permafrost in Iceland is largely restricted to the mountains in the north and east (e.g. Etzelmüller et al., 2007). Nevertheless, slabs of subglacial sediment can, in certain cases, freeze to the underside of glacier snouts in southeast Iceland due to the penetration of the winter cold wave (cf. Krüger, 1995, Krüger, 1996; Evans and Hiemstra, 2005; Chandler et al., 2016a).

2.3. Previous landsystems research

Glacial landsystems research at Fjallsjökull has thus far been largely incorporated in studies of the active temperate landsystem of neighbouring Breiðamerkurjökull, with the glacial geomorphology of

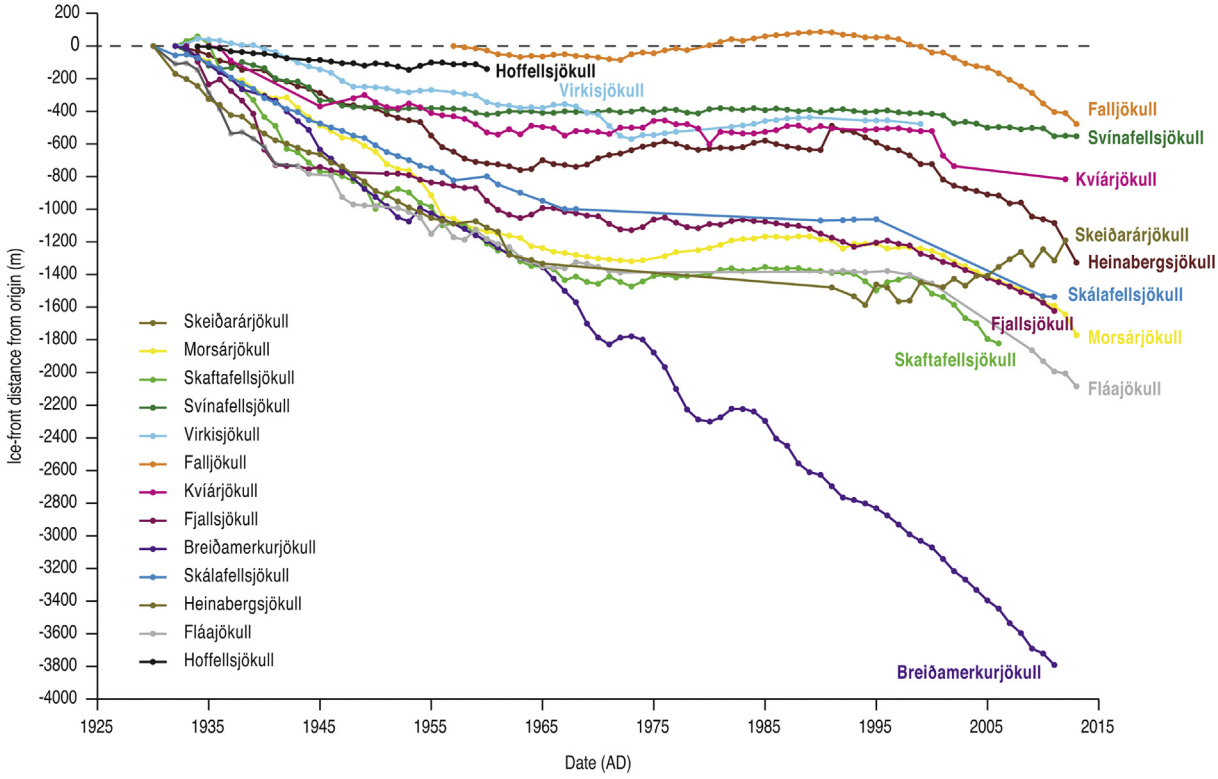

Fig. 3. Variations of the Öræfajökull and southern Vatnajökull outlet glaciers since 1931, compiled from ice-front measurements collated by the Icelandic Glaciological Society. Reproduced from Evans and Chandler (2018).

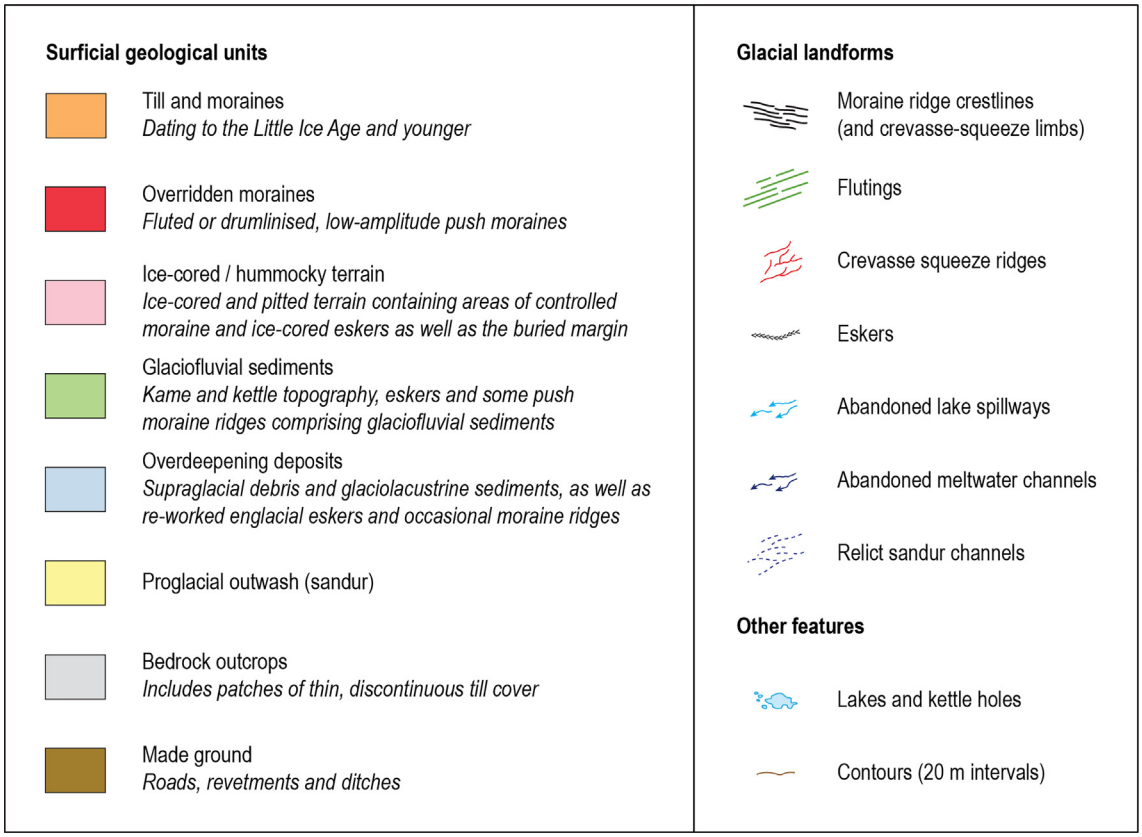

Fig. 4. Legend for all the glacial geomorphological maps (Figs. 5 and 6) presented in this paper and in the supplementary material. The symbology for the surficial geological units and glacial landforms follows the scheme widely applied to Icelandic glacier forelands (see Evans, 2009).

the Fjallsjökull foreland figuring partially in the University of Glasgow map series (Howarth and Welch, 1969a, 1969b; Evans and Twigg, 2002). Indeed, Fjallsjökull was not represented as an independent landsystem signature until the unfinished 1945 and 1965 maps were published much later by Evans et al. (2009), alongside a 1998 landsystems map. The foreland has been the target of several glacial sedimentological studies, focusing on particular elements of the landsystem (Price, 1970; Rose et al., 1997; Evans and Twigg, 2002; Evans and Hiemstra, 2005; Evans et al., 2018a). These studies include the development of the ice-marginal squeezing model for sawtooth moraine genesis (Price, 1970) and the submarginal-thickening till wedge model of moraine emplacement (Evans and Hiemstra, 2005; see also Evans et al., 2018a). Nevertheless, controls on the spatio-temporal evolution of the overall glacial landsystem signature at Fjallsjökull have received somewhat limited attention. Given this, and accelerated snout recession since 1998, there is a clear need for new landsystem mapping in order to understand the process-form response of Fjallsjökull to changing conditions (e.g. climate change, emerging basal topography) since the LIA.

3. Methods

3.1. Glacial landsystem mapping

Mapping of the glacial geomorphology and surficial geology of the Fjallsjökull foreland was undertaken following protocols outlined by Chandler et al. (2018), involving interpretation of remotely-sensed data and extensive field checking. We produced two glacial landsystem maps: (i) a small-scale (1: 15,000) map of the entire foreland based on airborne Light Detection and Ranging (LiDAR) data; and (ii) a large-scale (1: 2000) map of the glacial geomorphology at the southern margin based on UAV imagery.

The LiDAR data used to produce the 1: 15,000-scale map of the Fjallsjökull foreland (Supplementary Material 1) was collected in 2011 and 2012 by the Icelandic Meteorological Office and the Institute of Earth Sciences, University of Iceland (Jóhannesson et al., 2013). Digital Elevation Models (DEMs) with pixel sizes of 1 m and 2 m were interpolated from the raw LiDAR point clouds, which have horizontal and vertical errors of <0.5 m. As the 2012 LiDAR dataset does not provide complete coverage of the foreland, data from 2011 and 2012 were mosaicked together, and this is indicated on the final map. For the mapping, the DEMs were re-projected from ISN 2004/Lambert Conformal Conic 1993 (ESPG: 3057) to the UTM Zone 28 N (ESPG: 32628) reference system. Mapping was performed using hillshade relief models

Table 2
Summary of the UAV survey parameters and associated processing errors. Total (XYZ) root mean square errors (RMSEs), mean errors and standard deviation (SD) of error are reported relative to internal control points and external check points.

	Survey year			
	2016	2017	2018	2019
Survey date	09-2016	09-2017	08-2018	05-2019
Camera model	FC300S	FC6310	FC6310	FC300X
Survey area (km^2)	0.480	0.312	0.419	0.548
Average flight height (m)	71.8	86.0	89.8	86.6
No. of images	515	642	706	449
Ground sampled distance (cm/pix)	2.70	2.17	2.25	3.28
No. of control points	19	19	28	31
No. of check points	9	9	12	22
Total internal RMSE (cm)	9.46	10.27	13.75	4.56
Total external RMSE (cm)	17.07	12.30	17.32	5.79
Total internal mean error (cm)	8.89	9.17	11.13	2.12
Total external mean error (cm)	15.21	11.78	16.26	1.92
Total internal SD of error (cm)	3.33	4.75	8.22	5.01
Total external SD of error (cm)	8.22	3.78	6.24	6.08

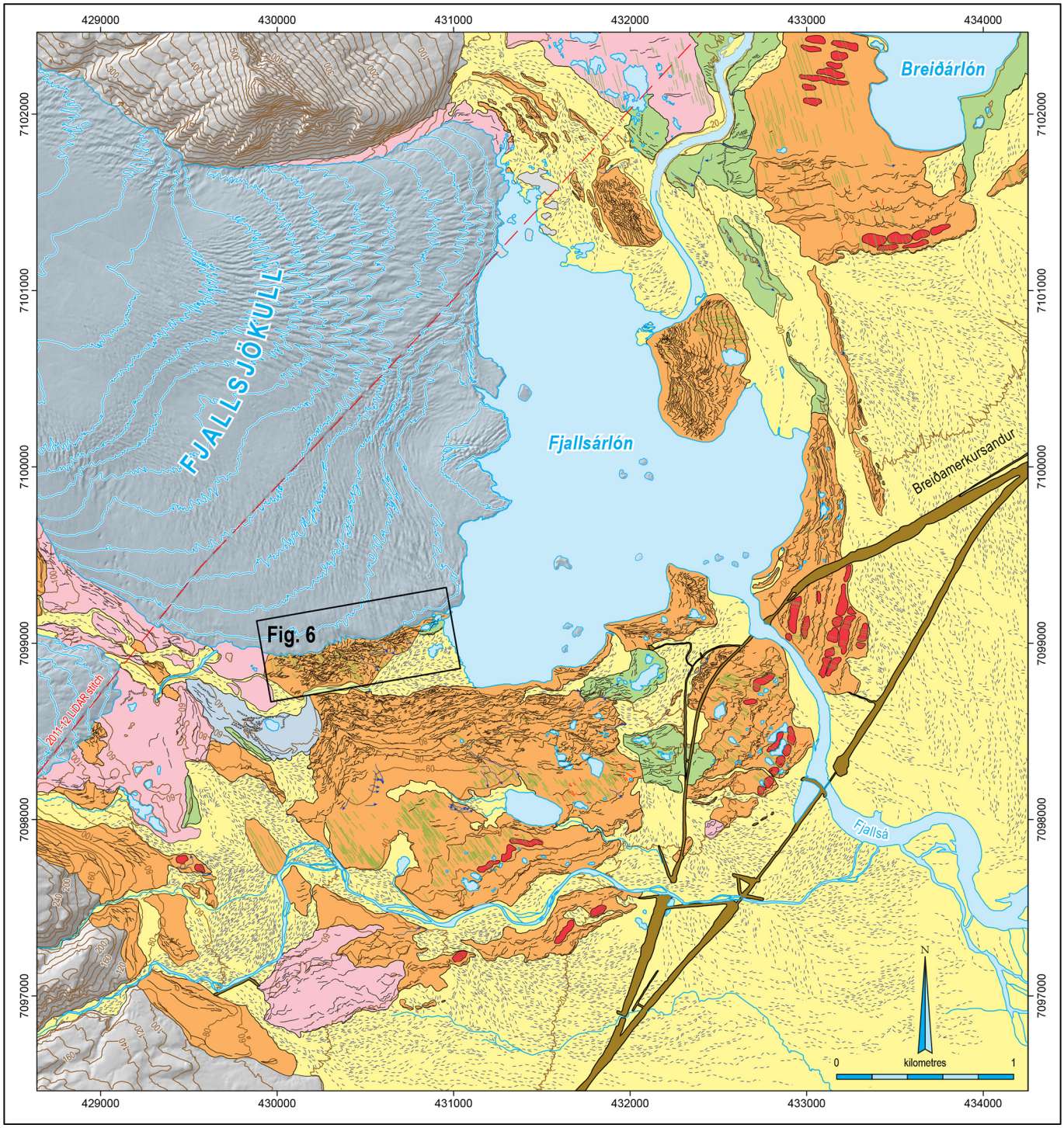

Fig. 5. Glacial geomorphological and surficial geological map of the Fjallsjökull foreland, depicting the sediment-landform assemblages of the glacial landsystem as they appeared in 2012. Data from 2011 and 2012 were stitched together (indicated by the red dashed line) to provide a composite DEM of the entire foreland. The location of our high-resolution UAV mapping is shown by the black frame. For key, see Fig. 4. A large format version of this map is available as Supplementary Material.

derived from the processed LiDAR DEMs. Additionally, historical aerial photographs (1945, 1965, 1982 and 1998) obtained from Landmælingar Íslands (the National Land Survey of Iceland) were consulted during mapping, along with 2015 Loftmyndir ehf aerial photographs that are available for viewing online (http://map.is/).

A 1: 2000-scale map of the glacial geomorphology and surficial geology at the southern Fjallsjökull margin (Supplementary Material 2) was produced using an orthophoto (3 cm per pixel) and a DEM (6 cm per pixel) derived from UAV imagery captured in May 2019. The imagery was captured over an area of ~0.5 km^2 using a DJI Phantom 3 Professional quadcopter, with the DJI GS Pro application used for programming autonomous flights (see also Chandler et al., 2020).

The interpretation of the remotely-sensed data was verified during field mapping campaigns, supported by sedimentological investigations of available natural exposures as well as sections created manually through specific landforms (see also Evans et al., 2018a; Chandler

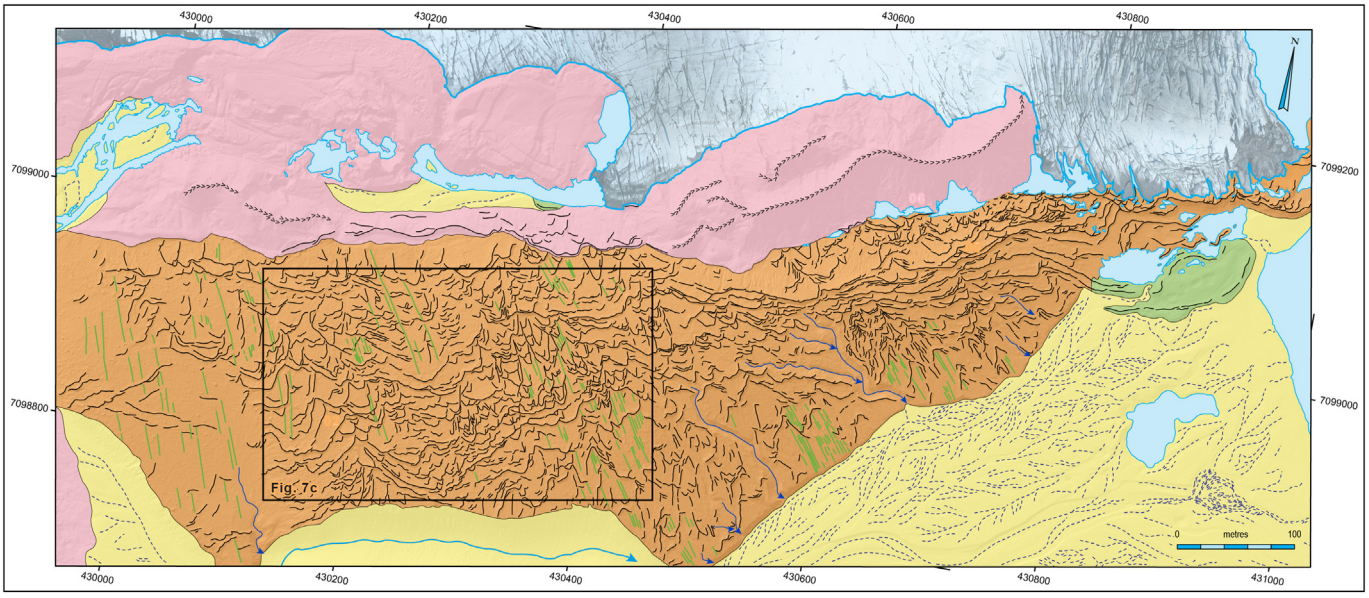

Fig. 6. Glacial geomorphological and surficial geological map showing the sediment-landform assemblages at the southern Fjallsjökull margin in May 2019 (see Fig. 5, for location). The mapping is based on interpretation of an orthophoto and a DEM derived from a UAV survey. For key, see Fig. 4. A large format version of this map is available as Supplementary Material.

et al., 2020). The sedimentological investigations followed standard procedures and involved logging and lithofacies analysis, as well as clast fabric and clast shape analyses (e.g. Evans and Benn, 2004; Lukas et al., 2013).

Mapping for both landsystem maps was performed digitally (i.e. through on-screen vectorisation) in ESRI ArcMap 10.5. Surficial geological map units and their characteristic landforms were mapped using the colour-coded scheme established at other Icelandic glacier forelands (e.g. Evans and Twigg, 2002; Bennett et al., 2010; Evans and Orton, 2015; Evans et al., 2016a, 2017a, 2017b). Contours (at 20-m intervals) were generated from the LiDAR DEM and overlain on the surficial geology before the vector data was exported from ESRI ArcMap to Adobe Illustrator for final map production. On the final small-scale, LiDAR-based map of the foreland, the mountain sides are depicted by an underlying LiDAR-derived hillshade. These areas primarily contain paraglacial deposits, residuum and exposed bedrock. Similarly, the glacier surface is represented by the LiDAR-derived hillshade to illustrate crevasses. On the large-scale, UAV-based map, the glacier surface is represented by a UAV orthophoto.

3.2. UAV surveying and data processing

Repeat UAV surveys were conducted in 2016–2019 at the southern Fjallsjökull margin (see Fig. 1) with the aim of capturing high-resolution aerial imagery to map and quantify recent landscape change. The UAV surveying and data processing followed a standard operational framework that has been applied in glacial environments elsewhere (see Ewertowski et al., 2019b). We conducted the surveys using lightweight, consumer-grade quadcopters (DJI Phantom 3 and 4), equipped with 12 megapixel and 20 megapixel fixed-lens cameras, respectively. The surveys yielded imagery with ground sampled distances (GSDs) of 2.17–3.28 cm per pixel (Table 2). Further specific details on our surveying strategy are described by Chandler et al. (2020).

The UAV-captured imagery was processed in Agisoft Metashape Professional Edition 1.5.3 using a semi-automated Python script (https://github.com/gisportsmouth/PhotoScan-Automation-Script; see also Schaefer et al., 2020). As part of the processing we implemented gradual selection to remove any outliers and highly erroneous points (see Chandler et al., 2020). Positional ground control for the UAV surveys was established in 2019 by surveying artificial targets with a Topcon HiPer V GNSS in post-processing kinematic (PPK) mode. The GNSS data were post-processed using RINEX data from the IceCORS network (National Land Survey of Iceland: https://www.lmi.is/en/icecors-network/) and then exported in WGS 1984/UTM Zone 28N (EPSG: 32628) format. For the 2016, 2017 and 2018 UAV models, positional information was established using GCPs generated from the 2019 UAV orthophoto (see Chandler et al., 2020). Using this method ensured that any errors associated with the GNSS surveying were minimized: using individual ground control surveys for each individual survey year would introduce additional external errors. The SfM processing yielded models with low (centimetre-scale) error values (Table 2) and high (millimetre to centimetre-scale) precision (Chandler et al., 2020). Checks on differences in height for selected stable areas also revealed distributions close to normal, suggesting random rather than systematic errors in the models. The final processed DEMs and orthophotos had GSDs of 0.04–0.06 m per pixel.

3.3. Quantifying landscape change

Landscape change was examined through 'DEM differencing' of downsampled UAV-derived DEMs (0.1 m per pixel). This method involves subtracting spatially-coincident raster grid cells from each other to produce DEMs of Difference (DoDs) (e.g. Tonkin et al., 2016). DEM differencing was performed using the Geomorphic Change Detection (GCD) plugin of Wheaton et al. (2010) in ESRI ArcGIS, a tool that has been applied in previous studies in glacial environments (e.g. Tonkin et al., 2016; Midgley et al., 2018; Ewertowski et al., 2019a). We applied a simple 'minimum level of detection' (minLoD) to each of the DoDs, calculated using error values that were derived from error assessments of the individual DEMs. This method assumes that the error within the DEMs is spatially uniform and discards any morphological changes below the minimum threshold. The statistical minimum LoD values were calculated using Eq. (1) (Brasington et al., 2003):

$$_{\min}LoD = t\left(\sigma_{Z1}{}^2 + \sigma_{Z2}{}^2\right)^{\frac{1}{2}} \quad (1)$$

where σ_{Z1} and σ_{Z2} are the vertical standard deviations of error for two DEMs. All morphological changes under this threshold are considered uncertain at confidence interval, t. In this study, a 95% confidence

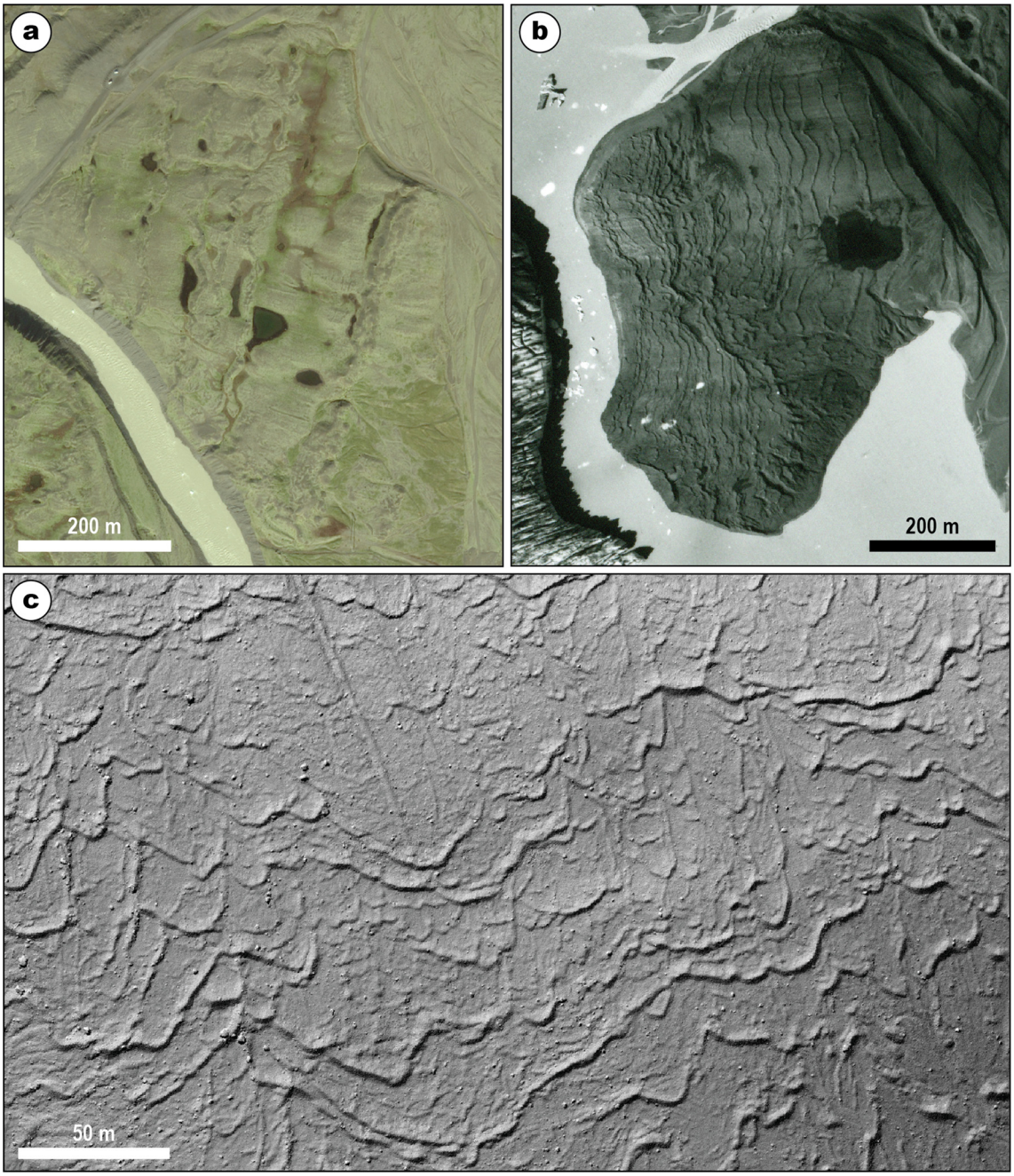

Fig. 7. Aerial imagery extracts showing variations in moraine planforms across the Fjallsjökull foreland. (a) Zones of smoothed and fluted moraine ridges (overridden moraines) with superimposed recessional moraines in the outer foreland. (b) Closely-spaced crenulated or 'sawtooth' moraines in the central part of the foreland. These moraines were constructed between the 1930s and 1960s, most likely on an annual basis (cf. Price, 1970). (c) Hillshade relief model extract showing an area of complex crenulated or sawtooth moraines near the southern Fjallsjökull margin (see Fig. 6). Note the long limbs of some moraines, which resemble the arms of hairpins.

interval was used; thus, under a normal distribution, $t = 1.96$ (Brasington et al., 2003; James et al., 2017; Cucchiaro et al., 2018). Vertical standard deviations of error were calculated for each of the DEMs using the vertical (z) error values between the models and the external checkpoints. Inputting these values into Eq. (1) yielded low minLoD values of 0.13–0.18 m.

4. Glacial geomorphology and surficial geology of the Fjallsjökull foreland

The surficial geological and glacial geomorphological maps of the Fjallsjökull foreland (Figs. 5 and 6; Supplementary Material 1 and 2) depict a foreland dominated by two surficial geological units that are characteristic of the active temperate glacial landsystem (cf. Evans and Twigg, 2002; Evans, 2003a, 2003b), namely (i) till and moraines and (ii) proglacial outwash (sandur). Within the former surficial geological unit, we identify (a) recessional moraines with distinctive crenulated or sawtooth planforms, (b) sets of minor flutings nested between individual moraine arcs, and (c) overridden moraines that are visible as broad, low-amplitude ridges with fluted/drumlinized surfaces. The proglacial outwash deposits (sandar) occur as either proglacial outwash fans beyond the LIA maximum limit, moraine-parallel ribbon sandur, or spillway-fed proglacial outwash fans. We also identified several other sediment-landform associations that form smaller components of the glacial landsystem, including localized areas of hummocky/ice-cored terrain, pitted kame and kettle topography, and eskers. Each of the

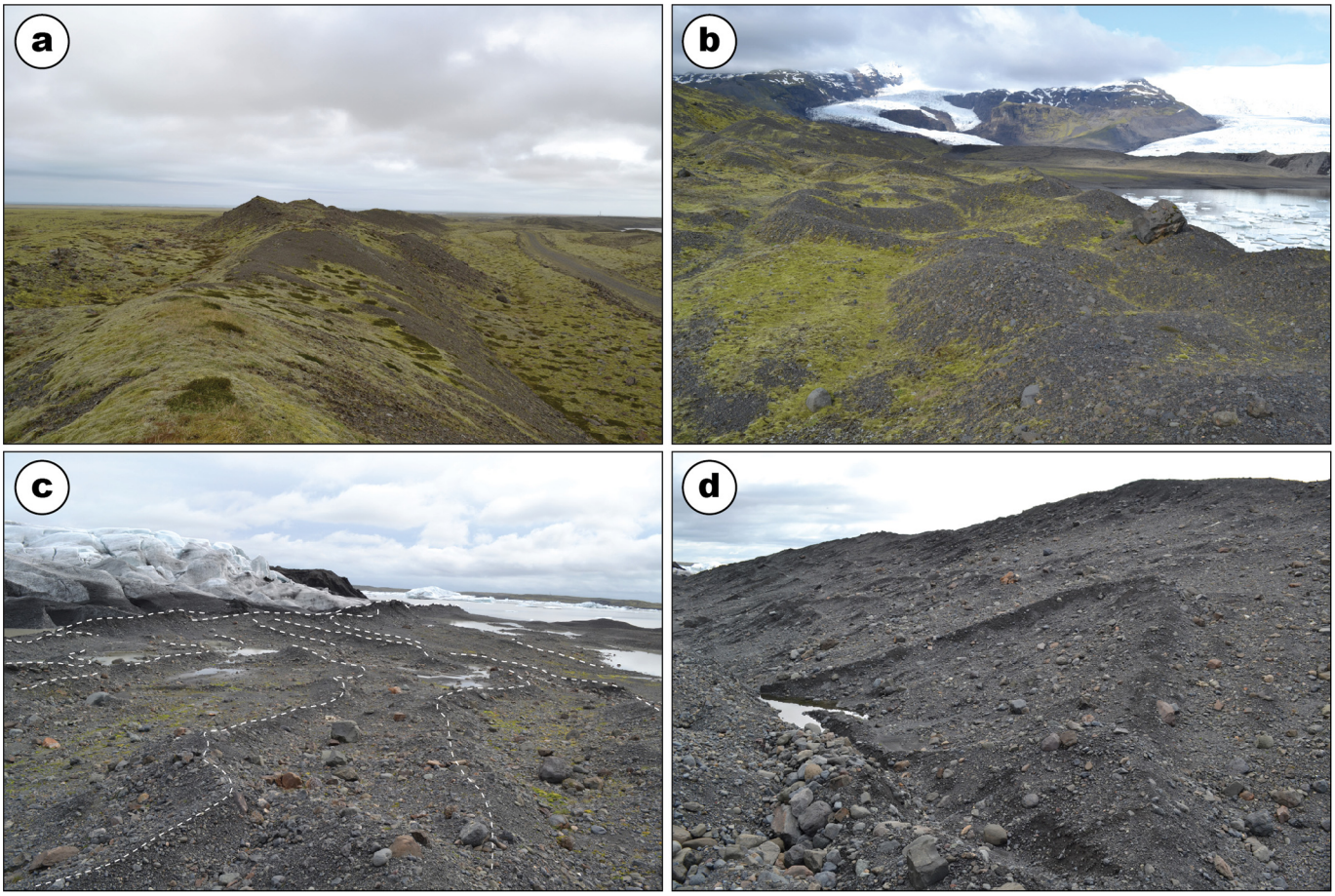

Fig. 8. Field photographs showing variations in moraine morphology across the Fjallsjökull foreland. (a) The large Little Ice Age moraine arc in the outer, eastern part of the foreland. (b) Superimposed moraines near the southeastern edge of Fjallsárlón. These moraines were constructed during the 1990s re-advance of Fjallsjökull. (c) Low-relief (<1.5 m high) sawtooth moraines near the present-day (2019) southern glacier margin, with moraine crestlines indicate by white dashed lines. (d) A small horseshoe-shaped moraine on the reverse slope near the southern margin. The moraine attains a maximum height of ~0.2 m.

surficial units and their constituent landforms are described in detail below.

4.1. Till and moraines

A significant component of the Fjallsjökull glacial landsystem is the till and moraine surficial geological unit, as is the case in all active temperate glacial landsystems in Iceland (Fig. 5) (cf. Evans and Twigg, 2002; Evans, 2003b). The till and moraine surficial unit is characterized by fluted subglacial traction till (cf. Boulton, 1987; Benn and Evans, 1996; Evans et al., 2010, 2016a, 2017a, 2018b, 2019a) and inset sequences of densely-spaced recessional moraines that frequently exhibit crenulated or sawtooth planforms (cf. Sharp, 1984; Boulton, 1986; Evans and Twigg, 2002; Evans et al., 2016a, 2017a; Chandler et al., 2016a, 2016b, 2016c; Everest et al., 2017).

Across the glacier foreland, from the LIA limit to the present-day glacier margin, there are notable changes in the morphology and planform arrangement of the moraines (Figs. 5, 7 and 8). In the outer part of the Fjallsjökull foreland, just inside the LIA limit, individual recessional moraines are relatively linear or gently undulating and can be connected together to form broadly arcuate chains of ridges that reach up to several hundred metres in length. These arcuate chains consist of moraine ridges that are ~5–185 m in length (average ~40 m) and 1–5 m in height. In the outer foreland, overridden moraines and sets of flutings occur between the individual chains of recessional moraines (Figs. 5 and 7a). The overridden moraines have broad (up to ~50 m wide), low-amplitude forms and display fluted/drumlinized surfaces. Overriding of the outer moraine arcs indicates that Fjallsjökull experienced an earlier Holocene advance of comparable magnitude to that of the LIA. This landform signature closely resembles those recognized at several outlet glaciers in Iceland, implying that the earlier Holocene advance was a regionally widespread phenomenon (cf. Krüger, 1994; Evans et al., 1999, 2016a, 2019a; Jónsson et al., 2014; Evans and Orton, 2015).

Further west/northwest, in the central parts of the Fjallsjökull foreland, there is a gradual transition to more complex, crenulated or sawtooth moraines (Figs. 5 and 7b) (cf. Price, 1970; Evans and Twigg, 2002; Evans et al., 2009). Individual ridges in these moraine fields typically attain heights of ~0.5–2 m, widths of ~4–10 m, and lengths of ~5–335 m. Their form can be extrapolated to form chains that extend for >1 km in some cases, with spacings of ~5–60 m between individual chains. The moraines become increasingly complex towards the present-day (2019), southern margin, where they display extremely sawtooth or ('hairpin-shaped') forms, and localized superimposition, cross-cutting and bifurcations are also evident (Figs. 6 and 7c) (Chandler et al., 2020). In several cases, the sawtooth moraines continue as, or are connected to, long ridge limbs (up to ~35 m) that are orientated obliquely to the moraine crestlines and sub-parallel to ice flow; this gives rise to moraine limbs that resemble the long arms of hairpins.

Sedimentological analysis of the small, sawtooth recessional moraines has revealed that they predominantly contain subglacial traction tills (with minor components of surface debris flow and glaciofluvial outwash cores), and have internal architectures and clast fabrics that are consistent with moraine construction by pushing and/or squeezing

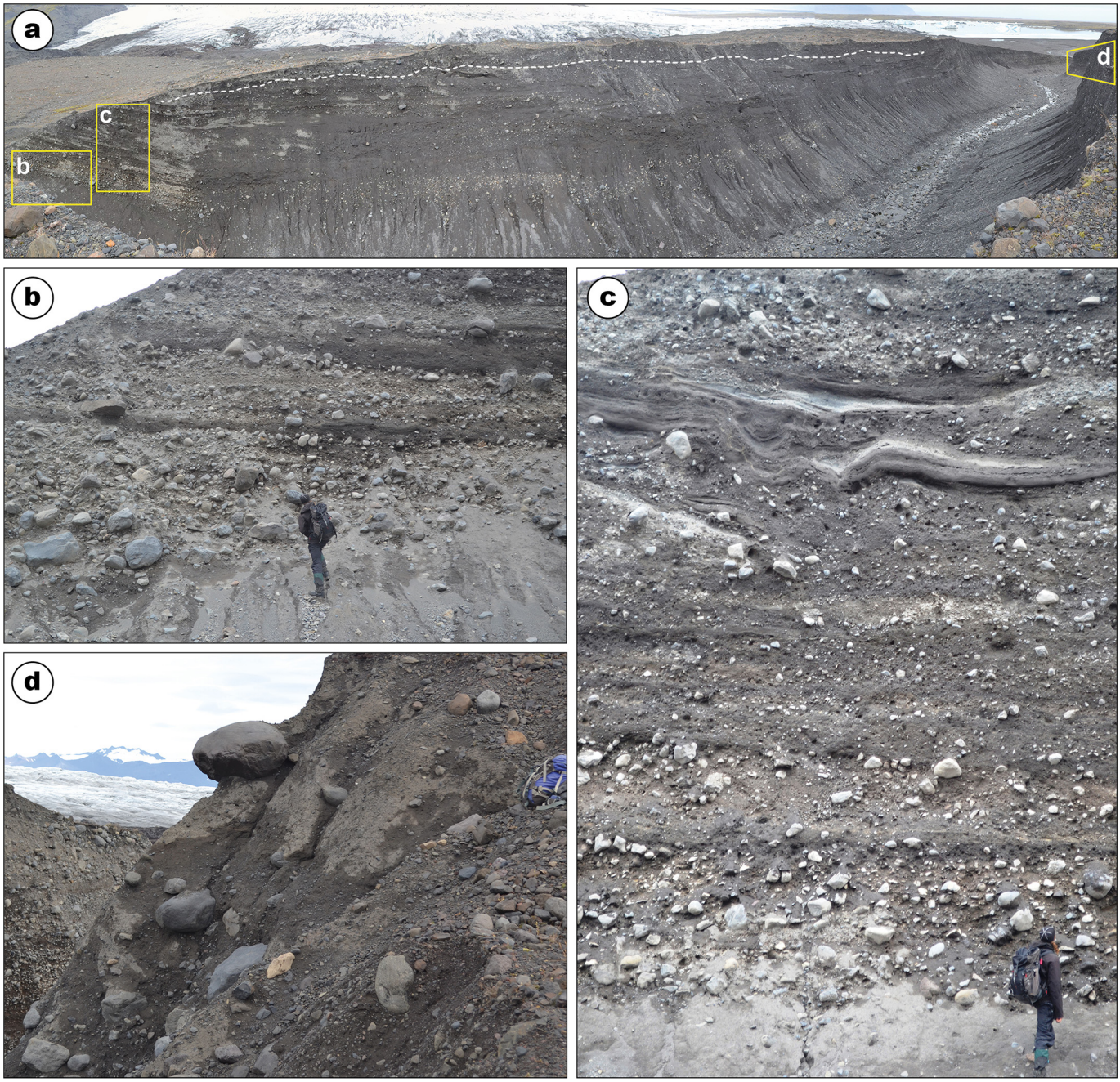

Fig. 9. (a) Overview photograph of the lake spillway in the southern Fjallsjökull foreland and (b–d) photographs of the exposed sediments, showing (b and c) horizontally-bedded outwash (boulder and cobble gravels) and discontinuous lenses of sands and silts with localized fold structures. The outwash sediments are locally capped by tills (d).

(Price, 1970; Roberts, 1995; Chandler et al., 2020). These recessional moraines can essentially be regarded as geomorphological expressions of the thickening of the subglacial deforming layer and production of glacier submarginal till wedges (cf. Evans and Hiemstra, 2005; Evans et al., 2018a; Chandler et al., 2020). The operation of this process-form regime at a glacier snout that is heavily indented by marginal radial crevasses (or pecten) gives rise to the distinctive sawtooth planform of the moraines found at Fjallsjökull and elsewhere in Iceland (e.g. Chandler et al., 2016a, 2016b, 2016c; Evans et al., 2016a, 2017a, 2019a). Specifically, squeezing of saturated subglacial tills through marginal crevasses/pecten, together with subsequent pushing, results in moraines that reflect the indented morphology of the glacier snout (cf. Price, 1970; Sharp, 1984; Chandler et al., 2016a; Evans et al., 2016a). By extension, the associated/connected long, ridge limbs also reflect infilling of the pecten by saturated subglacial tills (cf. Evans et al., 2016a, 2017a). The sawtooth moraines near the present southern Fjallsjökull margin are therefore best considered to be hybrid landforms, comprising push/squeeze moraines (outer wedges) that continue as crevasse-squeeze ridges (long ridge limbs) (cf. Evans et al., 2016a, 2017a; Evans and Ewertowski, 2018).

Locally, the till on the Fjallsjökull foreland thickens as sequences of multiple stacked diamicton units (Evans and Twigg, 2002; Evans and Hiemstra, 2005; Evans et al., 2018a). On the proximal slope of a substantial (up to 80 m high) arcuate ridge that runs through the middle of the foreland, Evans and Twigg (2002) reported a vertical succession of seven distinct diamicton units that are separated by discontinuous stratified units and/or clast pavements. They interpreted this sequence as stacked subglacial traction tills emplaced by NW-SE ice flow, as

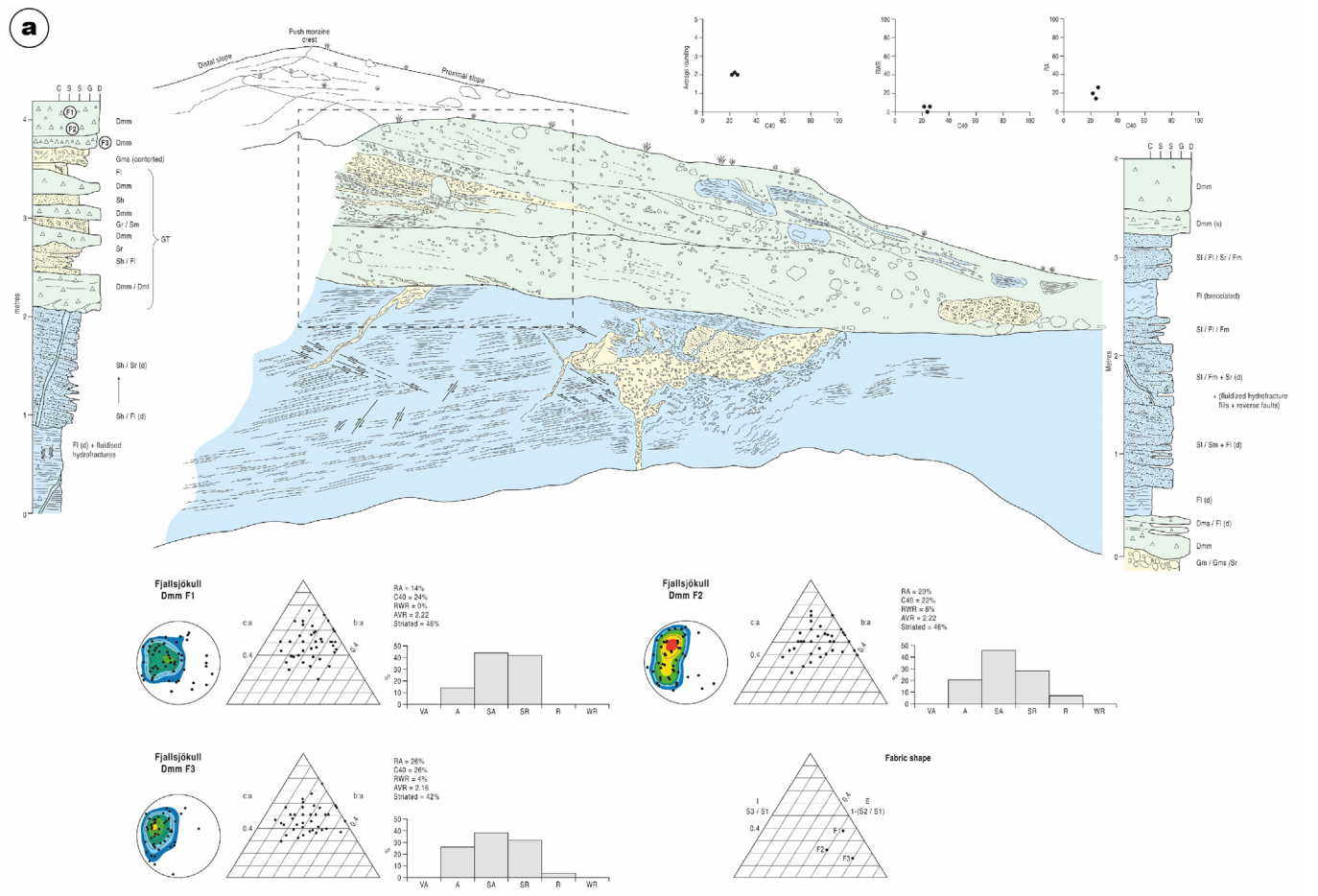

Fig. 10. (a) Scaled section sketch and vertical profile logs of an exposure in the middle Fjallsjökull foreland. (b) photographs of main exposure, showing the details of a vertical clastic dyke containing laminated silts and clays and a branching base, the stack of capping diamictons, and details (i and ii) of the nature of their internal fissile to crumbly structure. Sediments bracketed and labelled GT are classified as glacitectonite.
After Evans et al. (2018a).

indicated by clast fabric alignments that are consistent with the orientation of surface fluting. The large arcuate ridge itself contains glaciotectonized non-glacial sediments (lake infills of silts and fan gravels) and peat layers, with the organic detritus dating to the period 4.2–3.75 ka BP (Rose et al., 1997). Based on this evidence, Rose et al. (1997) proposed that this reflects widespread re-working of an older (mid-Holocene), large moraine ridge and associated proximal hollows during the advance of Fjallsjökull to its LIA maximum. More recently, catastrophic drainage of a proglacial lake at the southern glacier margin in 2003–2004 has incised an impressive gorge through the ridge, revealing a core of horizontally-bedded outwash that contains boulder and cobble gravels and discontinuous lenses of sands and silts with localized fold structures thought to be related to iceberg melt pits on a former sandur fan (Fig. 9) (Evans et al., 2018c). Thus, the ridge appears to represent a pre-LIA, glacially-overridden ice-contact fan/ramp, likely partially jökulhlaup-fed and locally capped by multiple tills.

Similarly, a glaciotectonite complex and multiple till units have been identified atop outwash sediments on the east side of Fjallsárlón (Fig. 10) (Evans et al., 2018a). The lower part of the sequence comprises poorly to moderately well-sorted cobble and pebble gravels with minor, discontinuous sandy gravel beds or lenses that are arranged in horizontal beds; these are representative of sheetflows that are typical of glaciofluvial outwash fans (sandar) found in southeast Iceland (Evans et al., 2018a). These outwash deposits are overlain by a massive diamicton and, in turn, a stratified diamicton, indicating a switch to ice-proximal subaqueous deposition. The diamicts are capped by sand, silt and clay rhythmites with dropstones that record sedimentation in a distal glaciolacustrine environment. Deformation structures (Riedel shears, hydrofracture fills) provide evidence for subsequent glacier overriding and glaciotectonization of the glaciolacustrine rhythmites (see Evans et al., 2018a, for further details). The sequence is capped by two diamicts that display characteristics typical of subglacial traction tills (cf. Evans et al., 2006, Evans, 2018). Vertical weakening of the clast macrofabric strengths through the diamicts appears to be representative of the A and B till horizons frequently found in southeast Iceland (cf. Boulton and Hindmarsh, 1987; Benn, 1995; Evans, 2000; Evans and Twigg, 2002).

Thicker till coverage at Fjallsjökull also occurs where larger composite moraines have been constructed by stacking of submarginal till units (Evans and Hiemstra, 2005). Internally, the composite moraines comprise upglacier-dipping, macroscopically massive diamictons (tills) that are separated by distinct partings or void spaces between upper and lower bounding planes; each till unit thins in an upglacier direction, forming till wedges. These composite moraines form by essentially the same processes as those that have constructed the small recessional moraines at Fjallsjökull (see above). However, submarginal thickening till wedges have been stacked at a relatively stationary glacier margin to form a composite ridge, as opposed to each till wedge manifesting as individual, discrete recessional moraines at an actively-retreating glacier margin (cf. Evans and Hiemstra, 2005; Chandler et al., 2016a, 2020; Evans et al., 2016b, 2018a). The stacking of multiple till units to form composite moraine ridges is a process-form regime that was observed

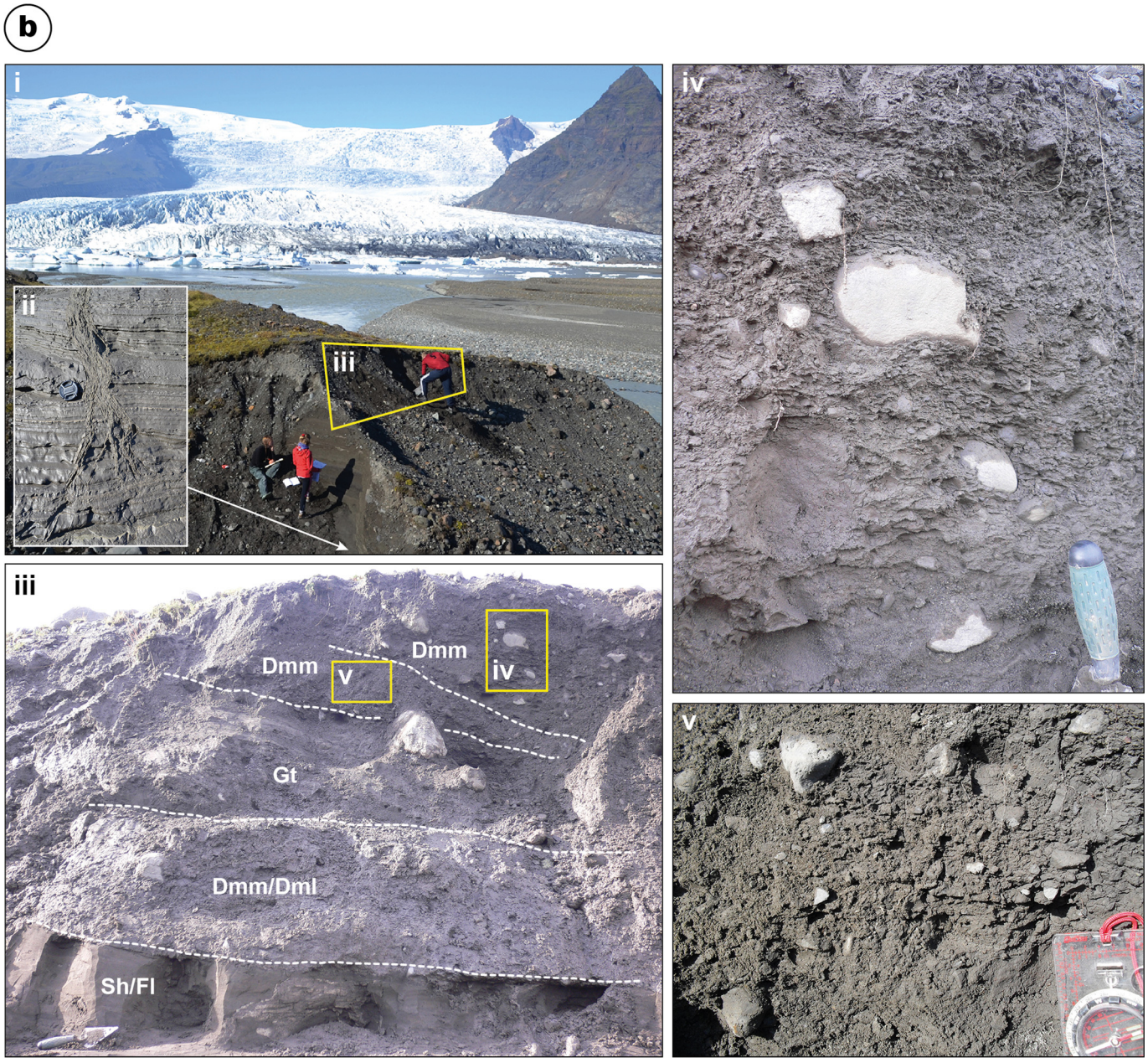

Fig. 10 (*continued*).

at many Icelandic glacier snouts during the early to mid-1990s, when a period of positive North Atlantic Oscillation (NAO) index values and long-term low annual air temperatures resulted in glacier snout re-advance and stabilization (cf. Sigurðsson et al., 2007; Evans and Chandler, 2018).

4.2. Ice-cored/hummocky terrain

Localized areas of hummocky terrain occur sporadically across the foreland, principally associated with former glacier suture zones that provided conditions conducive to hummocky moraine development (Fig. 5). Elsewhere on the foreland, the widespread development of chaotic hummocky moraine is precluded by the lack of appreciable supraglacial sediment cover, as is typical of active temperate glaciers (cf. Evans and Twigg, 2002; Evans, 2003a, 2003b). Northeast of Fjallsjökull, in the former coalescence zone with west Breiðamerkurjökull, there is a small area of fluted hummocks (Fig. 11). This fluted hummocky terrain is interpreted as glacially-overridden kame and kettle topography due to the gravelly nature of the deposits and the absence of a medial moraine on the 1945 aerial photographs (Evans et al., 2009). Additionally, the fluted hummocks are situated in a corridor of glaciofluvial sediments and esker ridges in the former Fjallsjökull–Breiðamerkurjökull suture zone (Fig. 5). Water-filled pits amongst the fluted hummocks reflect the melt-out and continued presence of buried glacier ice in the hummocky terrain, while the continuation of flutings across the water-filled pits indicates that overriding and streamlining occurred prior to pitting of the hummocky surface (Fig. 11).

Hummocky terrain is also evident in the outer, southern part of the foreland at the former site of a medial moraine between Hrútárjökull

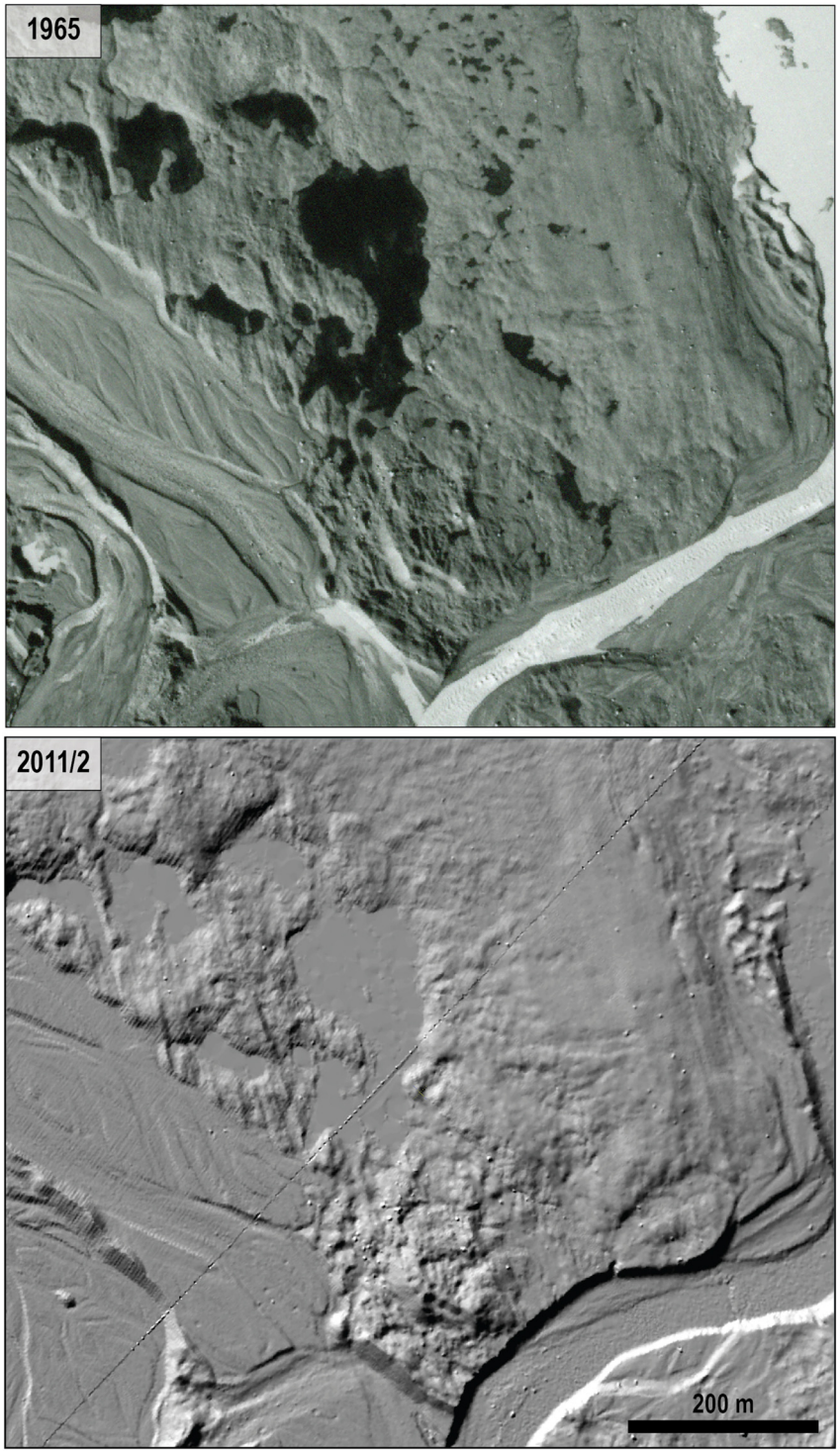

Fig. 11. Imagery extracts showing weakly fluted hummocky terrain on the northern foreland. The water-filled pits reflect the melt-out and continued presence of buried ice. Note the continuation of flutings on either side of the pits, indicating that overriding and streamlining occurred prior to pitting of the hummocky terrain.

and Fjallsjökull (Fig. 5). Comparison between repeat aerial photographs reveals that linear ridges within this area became increasingly fragmented over time (Fig. 12). The linear ridges can be traced to, or continue as, recessional push moraines on the adjacent fluted till surfaces, implying that these linear ridges also originated as push moraines. However, the gradual fragmentation of the linear ridges by the differential melting of the buried ice cores indicates that, where the ridges coincide with the former medial moraine, most of the debris was supraglacially derived. As a consequence of the supraglacial debris concentrated at this site, the former Hrútárjökull/Fjallsjökull medial moraine has retained linearity imparted by ice-marginal pushing.

Ice-cored/hummocky terrain is also evident at the southern sector of the present glacier margin (Figs. 5 and 6) where englacially-transported sediment emerged at the glacier surface during rapid recession and downwasting of the snout margin. The concentration of englacial debris at the snout, combined with rapid downwasting, resulted in burial of the glacier margin. Subsequent differential melting and degradation of the buried ice led to the development of hummocky/ice-cored terrain

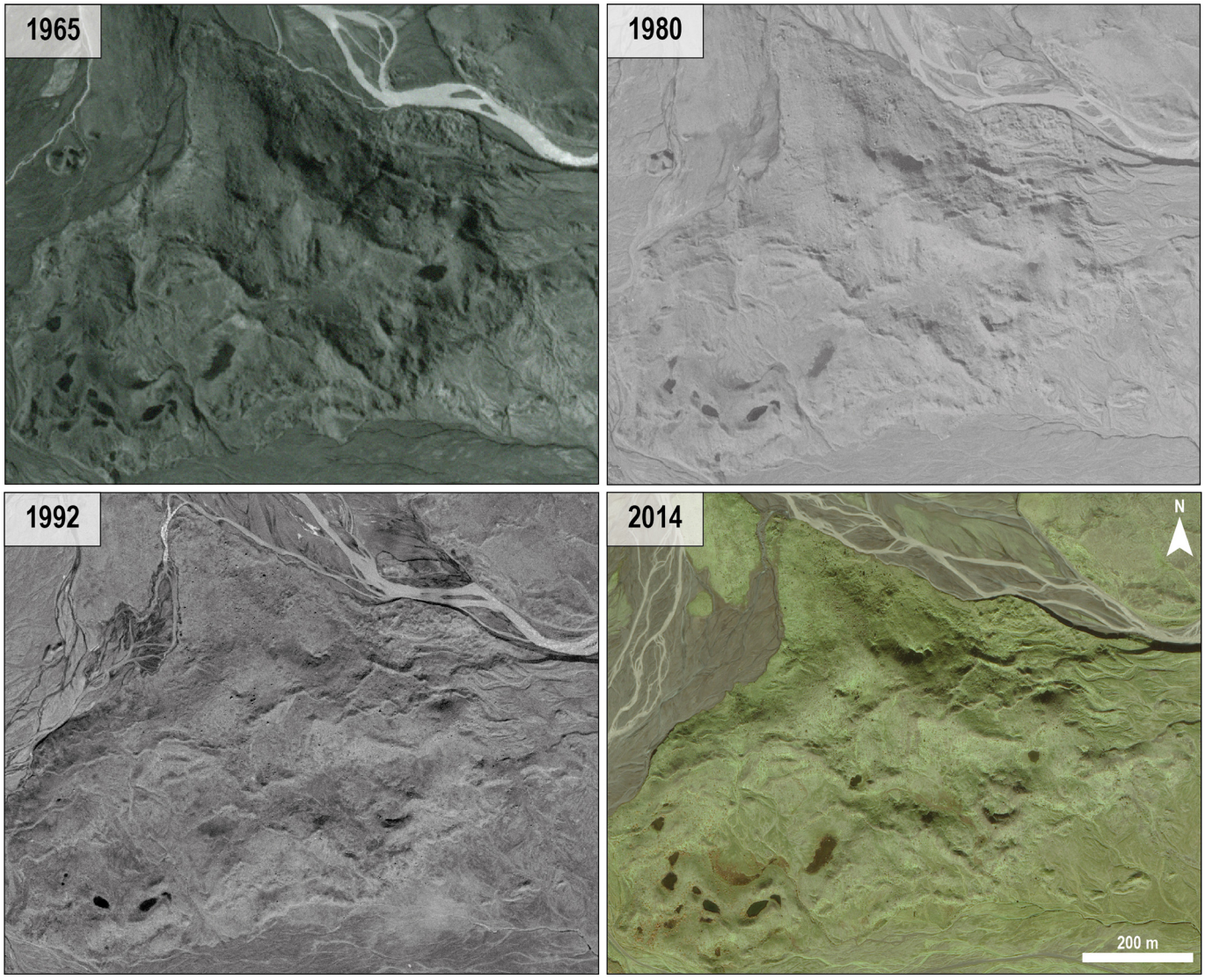

Fig. 12. Aerial imagery extracts showing the evolution of an area of hummocky terrain in the southern Fjallsjökull foreland. Melt-out of buried ice has resulted in the relief becoming more subdued, while discontinuous linear moraine ridges have become more fragmented.

and small pits. Additionally, the rapid thinning of the glacier snout has resulted in the emergence of former englacial conduit/tunnel fill deposits and the development of a substantial ice-cored esker (Fig. 6). These areas have been subject to substantial change in recent years and are considered in detail in Section 5, which presents our use of repeat UAV imagery to quantify recent ice-marginal landscape change.

4.3. Glaciofluvial deposits

The glaciofluvial landforms and deposits on the Fjallsjökull foreland are primarily contained within three assemblage types, namely proglacial outwash (sandur) fans, spillway-fed outwash fans or ribbon sandar (Fig. 13). Locally, ice-proximal outwash deposits also display prominently pitted surfaces, owing to ice meltout (Fig. 13b). These sediment-landform assemblages frequently occur on the forelands of active temperate glaciers in southeast Iceland (e.g. Price, 1969; Maizels, 1993; Marren, 2002, 2005; Evans, 2003a, 2003b; Evans and Orton, 2015; Evans et al., 2016a, 2017a, 2017b, 2019a).

The low-elevation terrain beyond the LIA maximum moraines enabled largely unimpeded proglacial drainage away from the glacier margin, leading to the accumulation of coarse-grained outwash gravels and sands as proglacial sandur fans (cf. Price and Howarth, 1970; Price, 1982; Evans and Twigg, 2002). The most expansive sandur fan deposits occur beyond the Fjallsjökull LIA maximum moraines, where a proglacial sandur fan was constructed by meltwater drainage emanating from the suture zone of Fjallsjökull and Breiðamerkurjökull (Fig. 13a). Progradation of this sandur fan occurred after 1904 and sometime prior to 1937 (cf. Price and Howarth, 1970). On the ice-proximal (western) side of the LIA maximum moraines, terraced ice-proximal outwash fan deposits are evident, incised by meltwater drainage from west Breiðamerkurjökull. Progradation and incision of these glaciofluvial sediments took place at some stage prior to 1945, by which time proglacial drainage had been diverted to the incipient Fjallsárlón. Continued evolution of the proglacial drainage network led to the coalescence of several sandur fans beyond the Fjallsjökull and Breiðamerkurjökull LIA moraines by 1945, producing the extensive (20 km wide and up to 5 km long) Breiðamerkursandur (cf. Price and Howarth, 1970). Esker ridges are also associated with the area of glaciofluvial sediments between Fjallsárlón and Breiðárlón (Fig. 13b), indicating that englacial and subglacial drainage was concentrated in the suture zone between Fjallsjökull and Breiðamerkurjökull.

Spillway-fed proglacial sandur fans and ribbon sandar form more minor components of the Fjallsjökull glacial landsystem signature. A spillway-fed proglacial outwash/sandur fan was constructed near the southern glacier margin in 2002–2004 (Figs. 7 and 13c). The

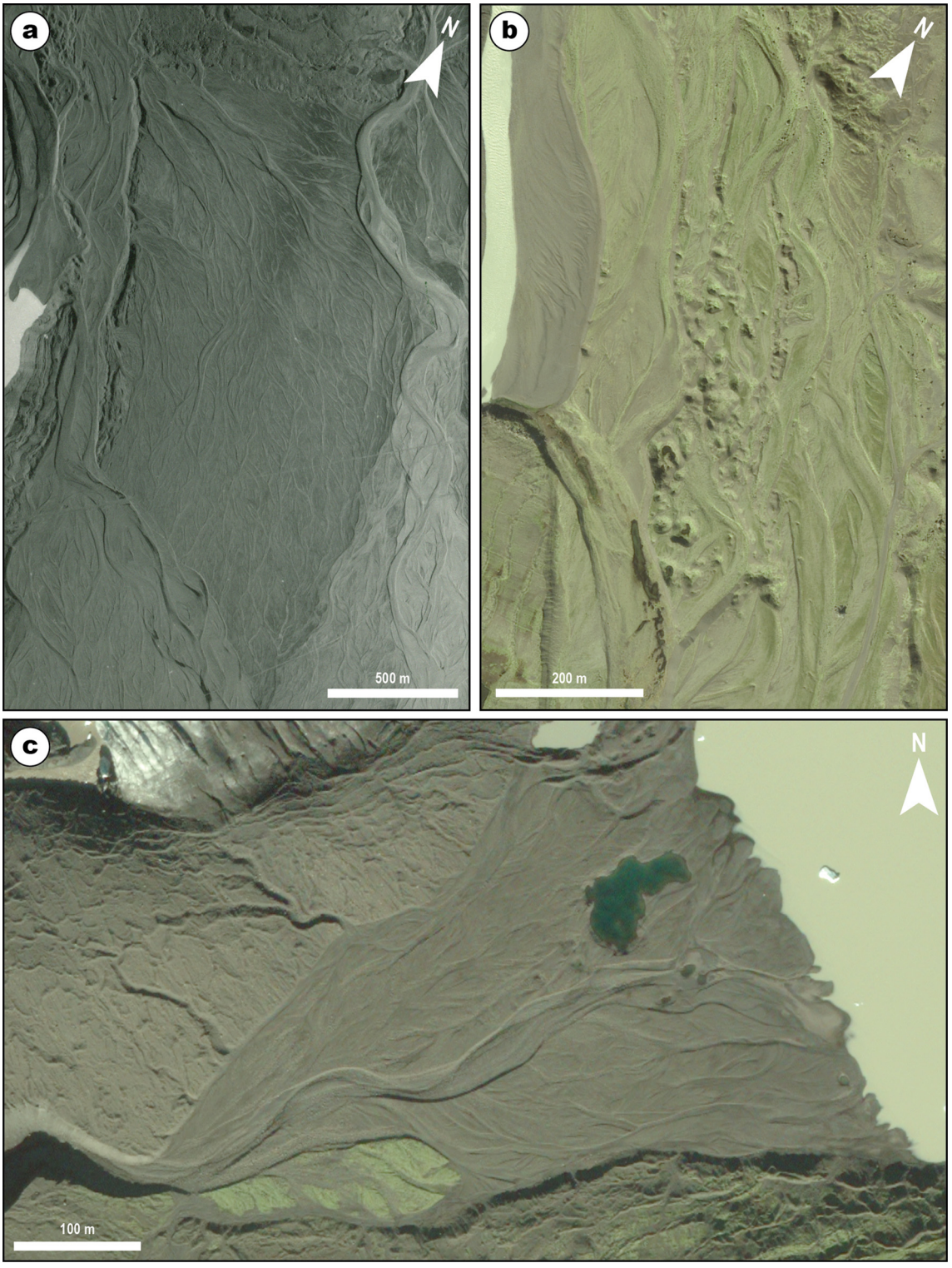

Fig. 13. Aerial imagery extracts showing examples of glaciofluvial sediment-landform assemblages on the Fjallsjökull foreland. (a) A proglacial outwash (sandur) fan at the former suture zone of Fjallsjökull and Breiðamerkurjökull. Also evident are channelized and terraced outwash deposits on the ice-proximal (western) side of the Fjallsjökull Little Ice Age moraine arc. (b) Terraced and pitted proglacial outwash tract constructed on the ice-proximal side of the maximum LIA moraines by meltwater emanating from western Breiðamerkurjökull. (c) A spillway-fed proglacial outwash (sandur) fan at the southern glacier margin.

progradation of this fan was associated with discharges emanating from the spillway that was incised through the large glacially-overridden ice-contact fan/ramp (see Section 4.1) during catastrophic drainage of a former lake. Localized ice margin-parallel outwash tracts have been formed were drainage was channelized between proglacial topographic high points (e.g. recessional moraine arcs) and the retreating glacier margin. Channelized linear/ribbon sandar occurs on the ice-proximal sides of the LIA moraine arcs (in the eastern and southern parts of the foreland), and between push moraine complexes on the north foreland (Fig. 5).

Glaciofluvial sediments also manifest on the foreland as kame and kettle topography, within which there are some very large (up to

~11,000 m^2) kettle holes (Figs. 5 and 14). Such large kettle holes are scarce in active temperate glacial landsystems, and the examples at Fjallsjökull are particularly unusual in that they are associated with push moraines on both sides of the depressions (Fig. 14). Significantly, the kettle holes shown in Fig. 14 are associated with elevated ice margin-parallel outwash tracts (ribbon sandar) that bend around the margins of the depressions. The relative spatial relationships between these sediment-landform assemblages indicate that the kettle holes represent the melt-out of snout ice that was buried by proglacial outwash. Moreover, the push moraines provide evidence for contemporaneous bulldozing of the glaciofluvial sediments during active glacier retreat. These processes resemble the situation at the debris-charged snout of Kviárjökull, although the sediment-landform assemblages at Fjallsjökull are not linked to incremental stagnation (cf. Bennett et al., 2010; Bennett and Evans, 2012).

4.4. Overdeepening deposits

Following the drainage of a former proglacial/supraglacial lake at the southern Fjallsjökull margin in 2003–2004, an important sediment-landform assemblage has been revealed. The floor of the depositional overdeepening is characterized by a complex assemblage of ice-cored, formerly englacial eskers (Fig. 15), the crestlines of which arc sequentially eastwards towards the deep lake spillway that traces to a spillway-fed proglacial sandur fan (see Section 4.3). The spatial patterns exhibited by the eskers record the evolution of the englacial drainage system during spillway incision: the curvature of the englacial conduit/tunnel fill deposits (eskers) indicates that the englacial drainage conduits migrated towards the spillway. Migration of the englacial drainage most likely occurred after drawdown of the lake and abandonment of the tunnel feeding the proglacial sandur fan. Significantly, the ice-cored nature of all the eskers in the depositional overdeepening provides evidence for englacial drainage bypassing the overdeepening, with englacial drainage only approaching the bed once the spillway had incised to its present level. The development of this localized, azonal landsystem signature (cf. Evans, 2013) provides important information on the development of meltwater drainage characteristics in relation to overdeepenings (Evans et al., In prep.).

5. Recent evolution of glacial landsystem signatures at Fjallsjökull

Between our 2012 and 2019 mapping of the Fjallsjökull foreland, substantial glacier retreat and volume loss occurred at the southern, land-terminating ice margin, along with concomitant ice-marginal landscape change (Fig. 16). Differencing between the 2012 LiDAR-derived DEM and the 2019 UAV-derived DEM reveals average surface lowering of ~19 m inside the 2012 glacier limit. Elevation changes range from −46 m to 8 m, with the areas of elevation increase linked to the development and migration of a substantial ice-cored esker at the southern ice margin (Fig. 6). While some areas exhibit surface increases, 94% (231,666 m^2) of areas with detectable change (i.e. those above the minLOD of 0.98 m) displayed surface lowering. Overall, recession and thinning of the snout zone shown in Fig. 16 resulted in net volume loss of 4,430,555 m^3 between 2012 and 2019, occurring across a total area of 245,692 m^2. Conversely, large parts of the UAV survey area (~52%) showed no detectable change between 2012 and 2019; these stable areas on the southern part of the foreland are characterized by low-amplitude recessional moraines and outwash fan deposits (Fig. 16). To illustrate the process-form response to recent retreat and thinning of the southern glacier margin, we now present three case studies based on repeat UAV surveys from 2016 to 2019.

5.1. Case Study 1: Evolution of ice-cored terrain

The first case study ('Area 1') is located on the western side of the UAV survey area (see Fig. 16) and contains significant proportions of buried ice. Of the three case studies, this area has undergone the most change. The DoDs reveal substantial surface lowering (Fig. 17) and volume loss in Area 1, with the greatest average surface lowering occurring between 2016 and 2017 (average lowering: ~0.5 m per month). Similarly, the DoDs indicate the majority of the volume losses occur between 2016 and 2017, with an average volume loss of ~20,406 m^3 per month across Area 1 (total area: 66,711 m^2). Volume loss in the subsequent survey interval (2017–2018) decreased considerably, with average volume losses of ~6330 m^3 per month across Area 1. Average volume losses were also reduced between 2018 and 2019 (~1326 m^3 per month), although the 2019 imagery was captured at the start of the melt season (May). Despite areas of elevation increase in 2017–2018 (Fig. 17b) and 2018–2019 (Fig. 17c), Area 1 mainly experienced substantial net surface lowering during the survey period (Fig. 17d). We anticipate that further surface lowering and volume loss occurred over the 2019 melt season, following the end of our UAV survey period in May 2019.

The surface lowering and volume loss recorded by the DoDs for Area 1 (Fig. 17) are largely accounted for by the rapid collapse of the glacier snout in this area. Elsewhere in Area 1, considerable surface lowering and volume loss in the DoDs reflects the degradation and meltout of buried ice by a combination of backwasting and downwasting (cf. Krüger and Kjær, 2000; Kjær and Krüger, 2001). Meltwater activity may have also contributed to degradation of the buried ice by oversteepening slopes and triggering slope failure (cf. Etzelmüller et al., 1996; Krüger and Kjær, 2000; Lukas et al., 2005). Additionally, de-icing processes and remobilisation of the sediment cover led to modification of ice-cored moraines near the glacier margin by mass movement and slumping, resulting in southwards migration of the ice-cored moraine complex (Fig. 18).

5.2. Case Study 2: Emergence and evolution of an ice-cored esker

The second case study ('Area 2') focuses on an ice-cored esker at the glacier margin, which emerged after 2014 (Fig. 19). The ice-cored esker gradually increased in volume between 2016 and 2019, with significant development in its form and surface elevation (Fig. 20). Detectable changes are evident in >80% of Area 2 throughout the survey period (2016–2019), with increases in surface elevation occurring across an area of 30,566 m^2 (~60% of the total area). In each survey year, volume increases are revealed by the DoDs, with average net increases across Area 2 of ~491 m^3 per month (2016–2017), ~7090 m^3 per month (2017–2018) and ~6337 m^3 per month (2018–2019). Changes in the surface form and elevation of the esker occurred in association with these volume changes (Fig. 20e and f). Between September 2016 and May 2019, surface elevation increased and distinct ridge crestlines formed, which are most clearly shown in Fig. 20f. Both transects display southwards migration of the ridge crestlines, with the ridge crestline migrating southwards by ~40 m between September 2017 and May 2019 along transect C–D (Fig. 20f).

The morphological changes detected on the DoDs (Fig. 20) record the continued emergence of a former englacial conduit/tunnel fill (esker deposits) and evolution of the ice-cored esker. This part of the glacier surface was debris free in 2014 (Fig. 19a), but retreat and thinning of the glacier led to a former englacial conduit/channel fill appearing at the glacier surface by 2016 (Fig. 19b). Sustained retreat and thinning of this part of the glacier margin between 2016 and 2019 allowed the continued build-up of the former englacial conduit fill (esker) at the surface (Fig. 19c–e). Ongoing ice flow, coupled with minor winter re-advances, resulted in southwards migration of the ridge crestline and the growth of the southern end of the ice-cored esker (Figs. 19 and 20).

The repeat UAV images and DoDs (Figs. 19 and 20) also identify changes to the ice-cored esker slopes, which reflect degradation of the buried ice and reworking of the sediments on the esker slopes. Meltout of the buried ice by backwasting and downwasting (cf. Krüger and Kjær, 2000; Kjær and Krüger, 2001), combined with the southwards

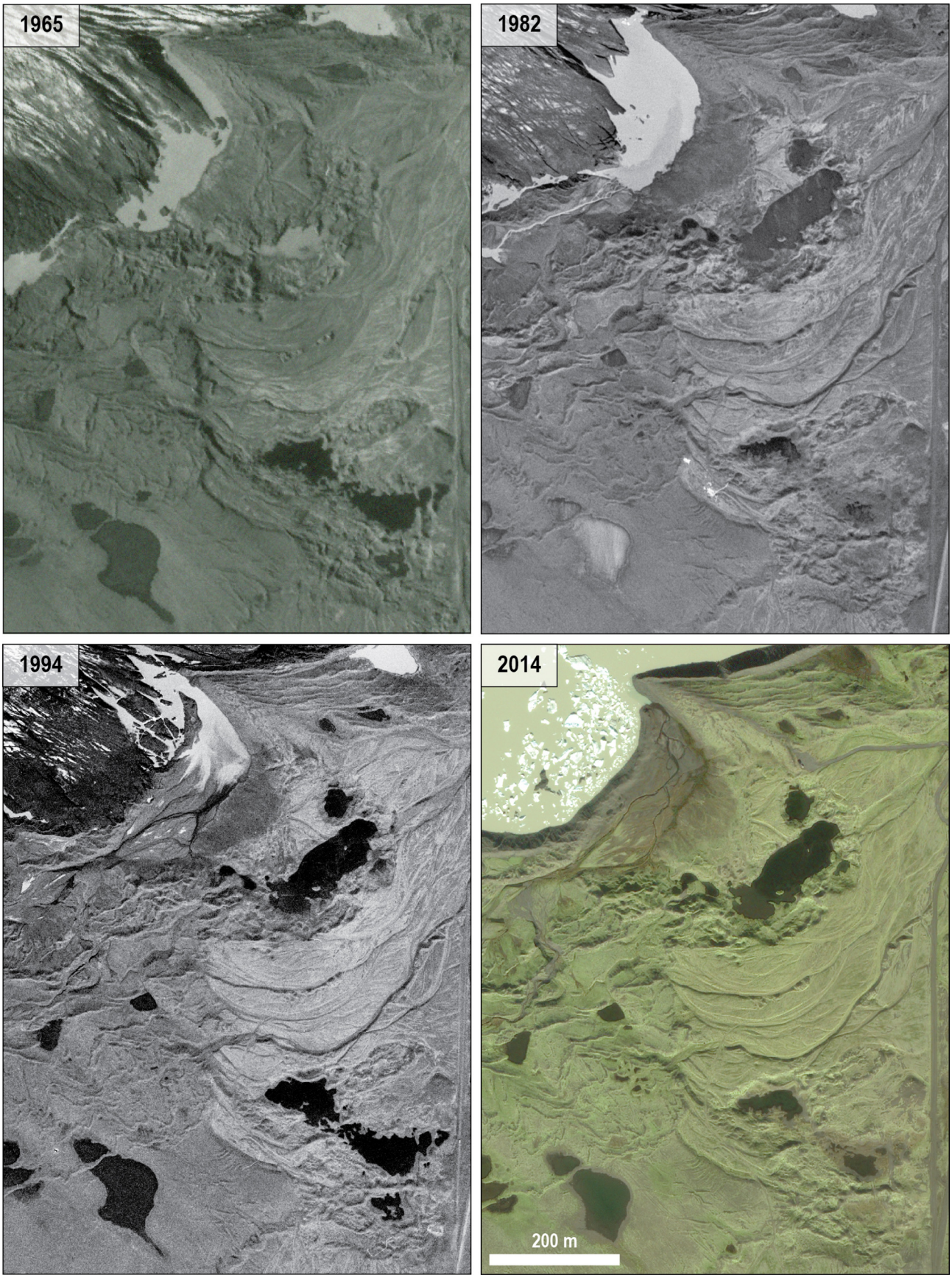

Fig. 14. Aerial imagery extracts showing the evolution of localized kame and kettle topography on the southern part of the Fjallsjökull foreland. Note the occurrence of push moraines on either side of the kettle holes, indicating that the kettle holes represent the melt-out of snout ice buried by proglacial outwash that was bulldozed during active glacier recession. The trend and elevated positions of the abandoned outwash tracts clearly show that the glacier snout occupied the depressions during outwash progradation.

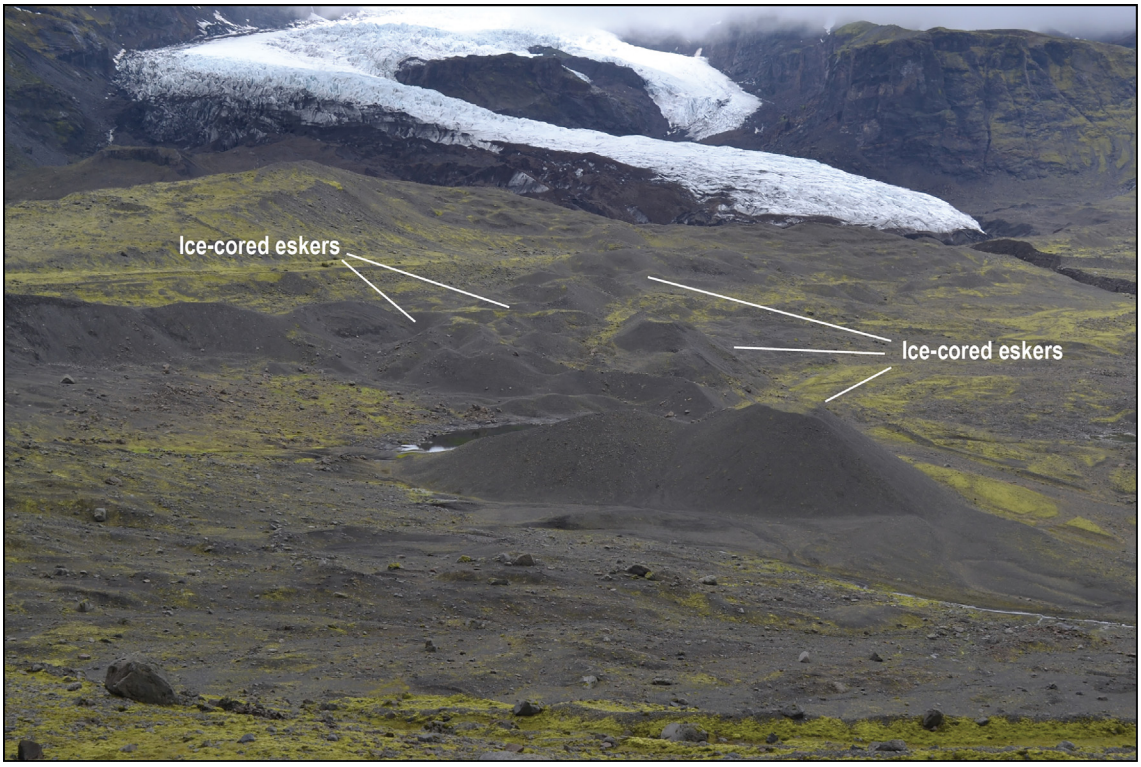

Fig. 15. Field photograph of ice-cored, formerly englacial, eskers in the depositional overdeepening of the southern foreland. The crestlines of the eskers arc eastwards (left to right) towards the deep lake spillway, documenting the evolution of the englacial drainage system during spillway incision.

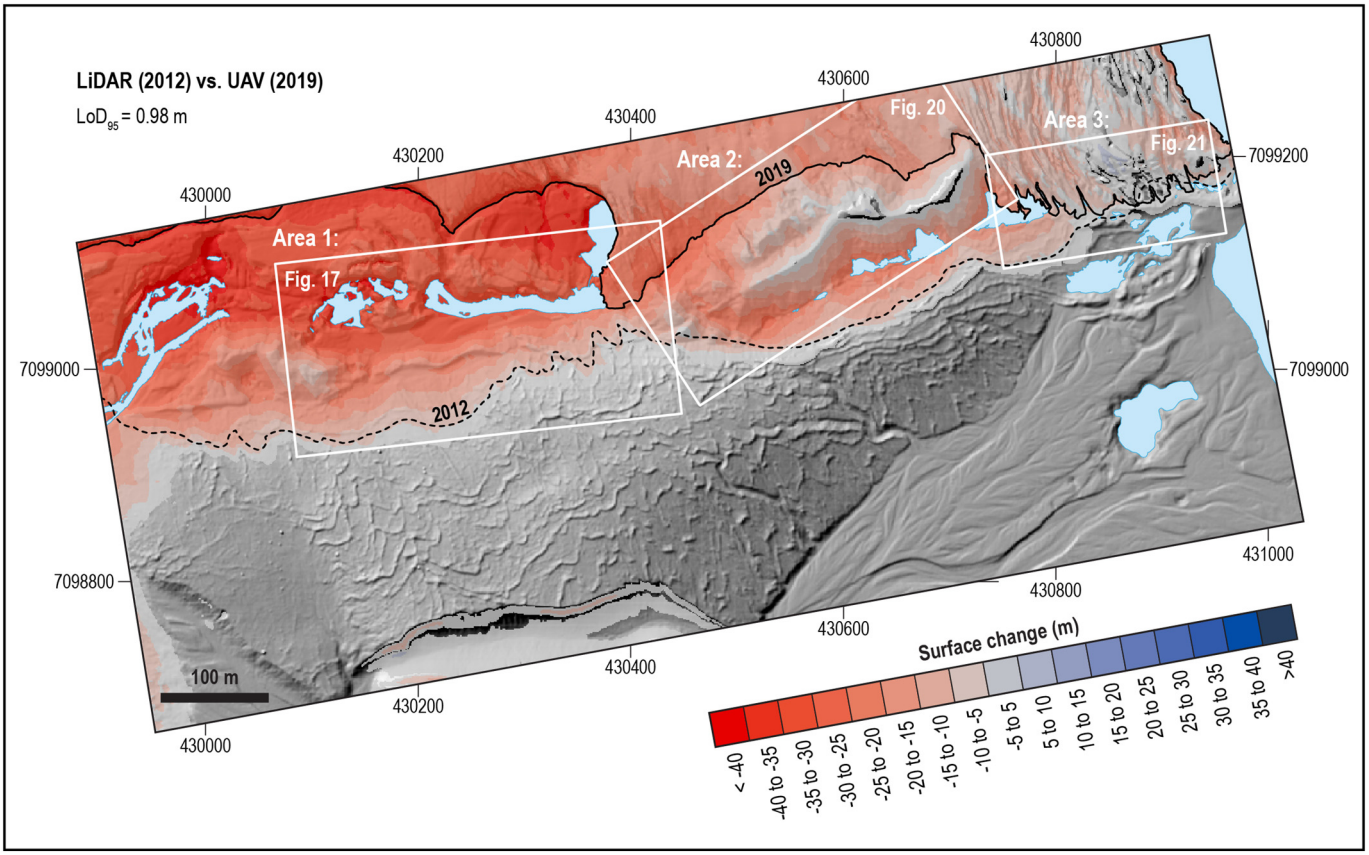

Fig. 16. DEM of Difference (DoD) for the 2012 LiDAR DEM and 2019 UAV DEM. Blank areas, where the underlying hillshade from 2019 is visible, represent areas with no detectable change (i.e. stable areas). The dashed (2012) and solid (2019) black lines show positions of the glacier margin. The blue polygons mask water bodies, which are not resolved by SfM photogrammetry. The white frames indicate the locations of case studies selected for more detailed analysis.

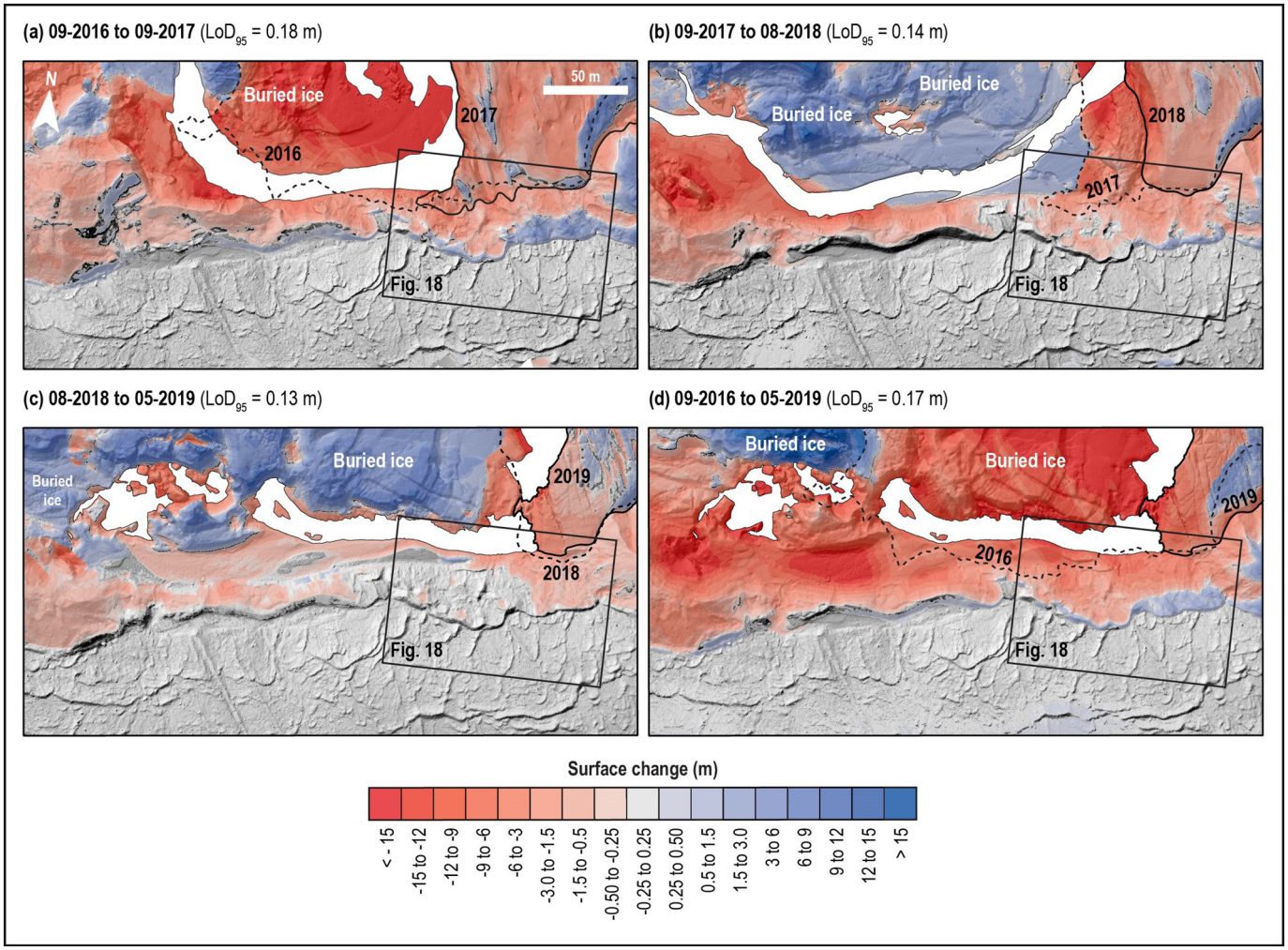

Fig. 17. DEMs of Difference (DoDs) for an area of ice-cored terrain (Area 1). Increases in elevation are indicated by blue colours, while decreases are indicated by red colours. Blank areas, where the underlying hillshade is visible, represent areas with no detectable change. The dashed and solid black lines show positions of the ice margin. Water bodies are masked by white polygons as they are not resolvable in SfM photogrammetry. Note, the 2019 UAV survey was conducted at the beginning of the melt season (May 2019), whereas the 2016–2018 surveys were undertaken towards the end of the melt season (August/September). For location, see Fig. 16.

migration of the esker, has led to the surface lowering visible in Fig. 20b and c. De-icing and remobilisation of the sediment also led to mass flows and slumping on the southeast-facing slope between 2018 and 2019 (Figs. 19 and 20c; Krüger and Kjær, 2000; Kjær and Krüger, 2001; Lukas et al., 2005; Schomacker and Kjær, 2007, 2008).

5.3. Case Study 3: Glacier recession and sub-annual moraine formation

Our third case study ('Area 3') focuses on the eastern end of the southern, land-terminating Fjallsjökull margin (see Fig. 16). DoDs for Area 3 reveal both positive and negative glacier surface changes, but with predominantly increases in elevation along the margin as well as in the immediately-adjacent, ice-marginal landscape (Fig. 21). Overall, the first two survey intervals reveal average volume losses of ~795 m^3 per month (2016–2017) and ~130 m^3 per month (2017–2018). In these two intervals, losses occur over areas of 8367 m^2 (~58% of the total area; 2016–2017) and 7839 m^2 (~51% of the total area; 2017–2018), respectively. The final survey period (2018–2019) exhibits an average volume increase of ~1671 m^3, but the most recent UAV survey (May 2019) was performed at the beginning of the melt season. The DoDs and transects across the DEMs show net advances of the glacier margin in each successive year, with the successive advances of the margin leading to the deposition and continued build-up of a ~4–5 m high moraine ridge (Fig. 21). This moraine is much larger than the ≤1.5 m high moraines that typify most of the surveyed area. Examination of the repeat UAV imagery reveals that the successive re-advances of the glacier margin have resulted in (a) superimposition of moraines and (b) complete overriding and destruction of moraines deposited in the previous year (Fig. 22). Furthermore, the UAV imagery captures multiple (3–6) moraines being formed in each year between 2016 and 2019 (see also Chandler et al., 2020). To our knowledge, this dataset of UAV-captured imagery provides the first unequivocal evidence of sub-annual moraine formation, with such high frequency moraine formation having only been identified in two previous studies at Icelandic outlet glaciers by counting moraines between bracketing ice-marginal positions (Krüger, 1995; Chandler et al., 2016a).

6. Spatial and temporal evolution of glacial landsystem signatures at Fjallsjökull

Based on our glacial landsystem mapping and assessments of aerial imagery, we recognize distinct landform patterns at Fjallsjökull and define three main landform zones, particularly relating to the nature of moraine and proglacial outwash deposition (Fig. 23). Landform zone 1, in the outer foreland, is characterized by (a) drumlinized and fluted, overridden moraine arcs and (b) proglacial outwash (sandur) fans. Landform zone 2, in the middle foreland, comprises closely-spaced and locally superimposed, sawtooth moraines that are concentrated

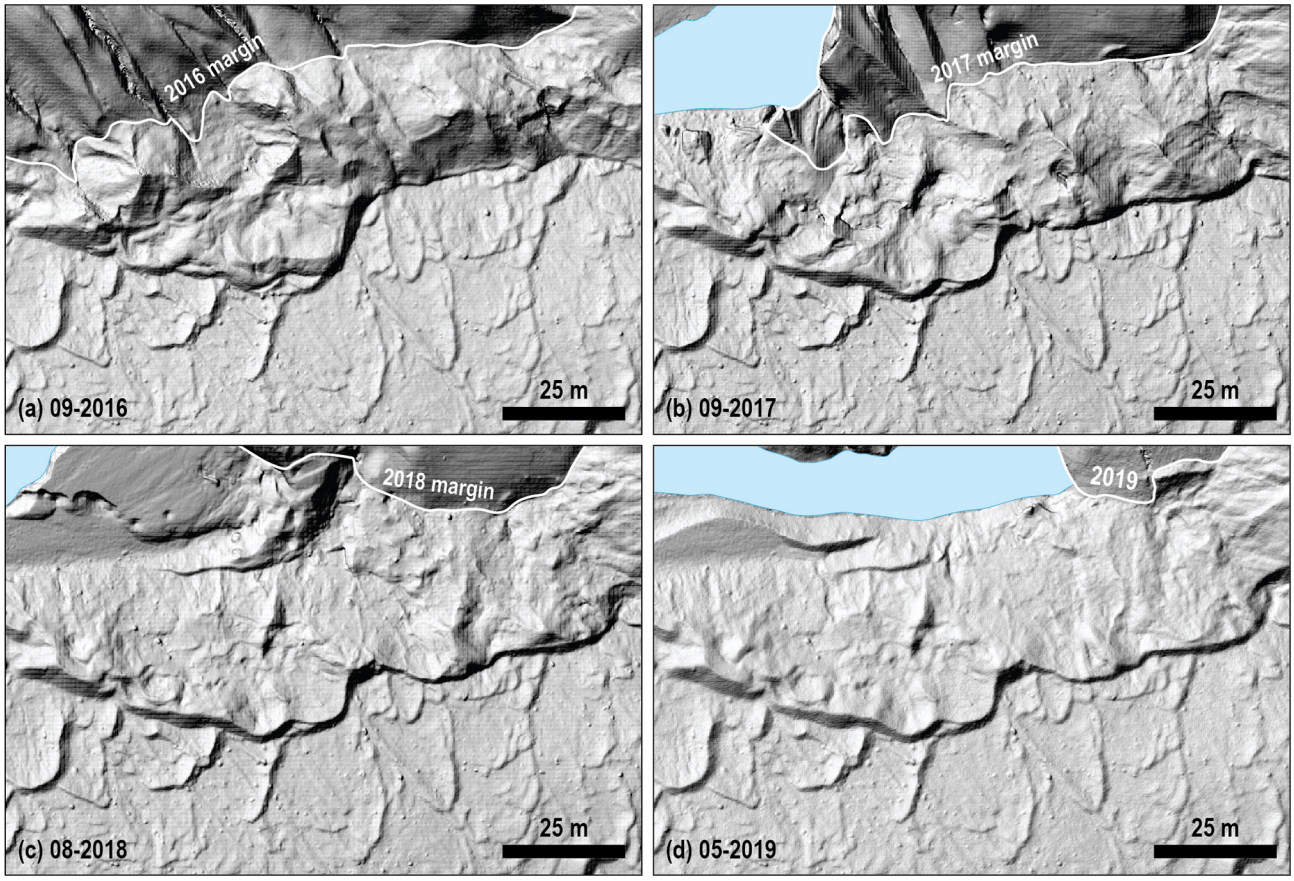

Fig. 18. Extracts from the hillshaded relief models for 2016–2019 showing the evolution of the ice-cored terrain and meltout of buried ice. Blue polygons mask water bodies. For location, see Fig. 17.

on topographic highs and were formed from ~1945 onwards (Section 4.1; Figs. 5 and 7a). Landform zone 3, at the southern glacier margin, is defined by a switch (in the early 2000s) to the production of multiple extremely sawtooth/hairpin-shaped moraines and associated crevasse-squeeze ridges per year (Sections 4.1 and 5.3; cf. Chandler et al., 2020).

The distinction between landform zones 1 and 2 at Fjallsjökull can be related to spatio-temporal changes in proglacial drainage characteristics and the structural architecture of the glacier snout during climatically driven glacier recession and thinning since the Little Ice Age (Fig. 23) (cf. Sigurðsson et al., 2007; Hannesdóttir et al., 2015; Evans et al., 2019b). Glacier recession from the outer LIA moraine arc would have resulted in a switch from uninhibited proglacial drainage and coupled glacier-glaciofluvial systems to comparatively poorer drainage conditions and increasingly topographically-controlled meltwater drainage (cf. Benn et al., 2003). This transition manifests in the glacial landsystem signature as a switch from the construction of proglacial sandur/outwash fans by unconfined meltwater drainage (landform zone 1) to channelized and terraced ice margin-parallel outwash tracts on the proximal side of the overridden moraine arcs (landform zone 2) (Fig. 23; see also Section 4.3). Importantly, in the context of developing modern analogues for ancient glacial landscapes, this change in proglacial drainage characteristics at Fjallsjökull is primarily determined by sediments deposited by the glacier itself, rather than by pre-existing bedrock topography. At the same time, a transition from compressive flow to increasingly extensional, divergent flow in the thinning glacier snout is suggested to have led to the development of radial marginal crevasses (Fig. 23). The combination of a relatively poor drainage conditions and a change to the crevasse architecture would have facilitated the formation of sawtooth push/squeeze moraines (see Section 4.1; Price, 1970; Evans and Hiemstra, 2005; Chandler et al., 2016a; Evans et al., 2016a).

The switch from sawtooth annual moraines (landform zone 2) to extremely sawtooth/hairpin-shaped sub-annual moraines (landform zone 3) most likely relates to a combination of elevated temperatures, high surface meltwater fluxes to the bed, and poor drainage conditions imparted by the depositional overdeepening (Section 4.1; Chandler et al., 2020). We suggest that above-average temperatures during recent years drove enhanced glacier surface melt and meltwater flux to the bed, saturating the subglacial sediments and elevating porewater pressures. Rapid conveyance of surface meltwater to the glacier bed near the snout margin may have been facilitated by an efficient (or 'fast') englacial drainage system (cf. Hart et al., 2015, 2019a, 2019b). The situation is exacerbated by the poor drainage conditions imparted by the emerging overdeepening, resulting in highly-saturated submarginal sediments and high porewater pressure. Together, these factors provided prime conditions for ice-marginal squeezing (cf. Price, 1970; Sharp, 1984; Evans and Hiemstra, 2005; Chandler et al., 2016a, and references therein). Increasingly divergent flow and pronounced marginal crevassing in response to glacier thinning are responsible for the exaggerated sawtooth/hairpin moraine patterns. While similar landform zones have been identified at other Icelandic outlet glaciers (e.g. Evans et al., 2016a, 2017a, 2019a), Fjallsjökull is the first outlet at which sub-annual moraine formation has been identified unequivocally. However, given the morphological similarities between the moraines and associated crevasse-squeeze ridges in landform zone 3 and those at other outlets in the region, we hypothesise that sub-annual moraines are a prevalent feature in the active temperate glacier landsystems of southeast Iceland.

In addition to the three main landform zones, we recognize localized (azonal/intrazonal) sediment-landform assemblages that are not

commonly found in active temperate glacial landsystems and reflect specific conditions found at Fjallsjökull. These localized sediment-landform signatures include fluted hummocky terrain (Fig. 11; Section 4.2), kame and kettle topography (Fig. 14; Section 4.3), and a unique assemblage of formerly englacial, ice-cored eskers in a depositional overdeepening (Fig. 15; Section 4.4). Most significantly, our

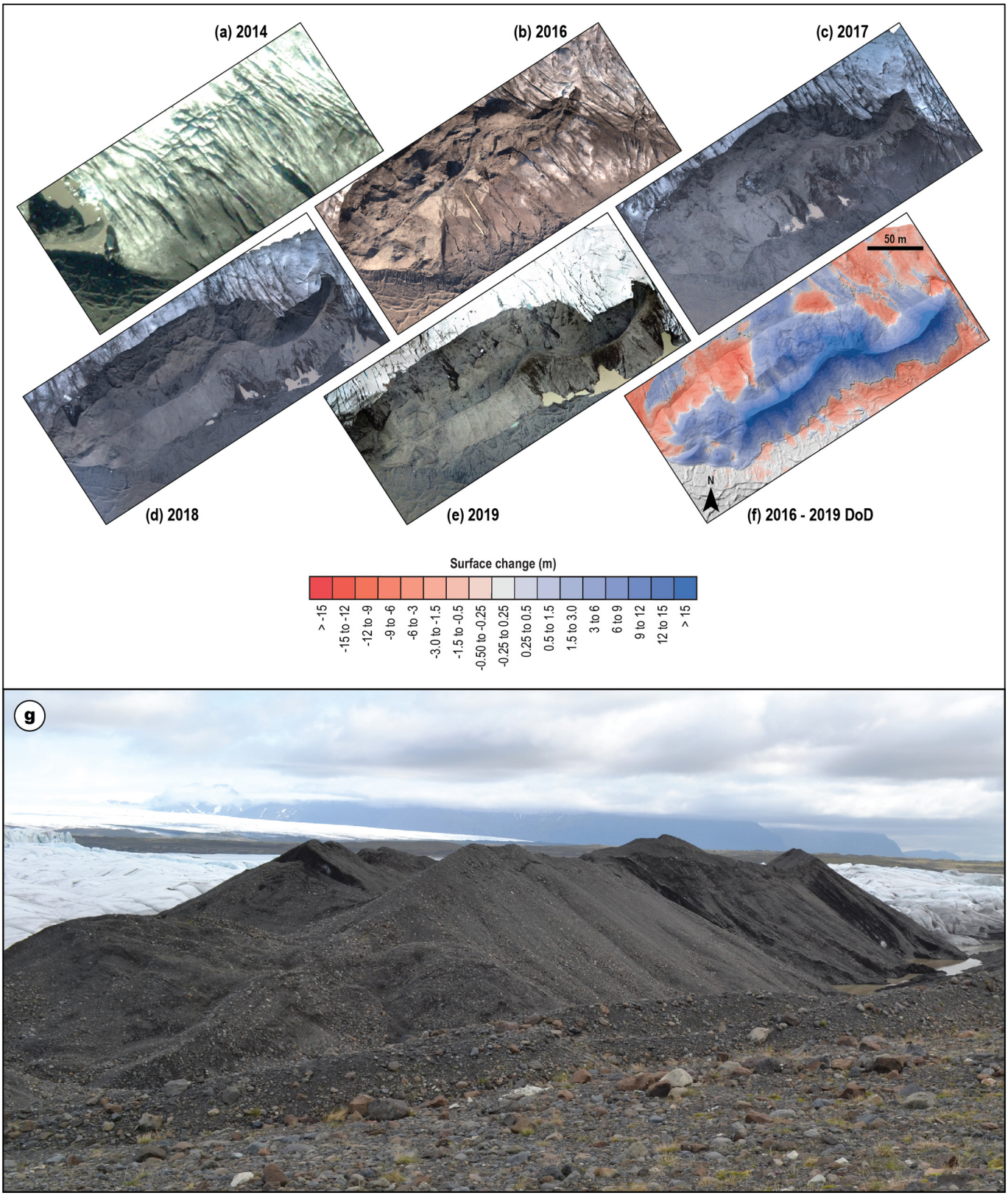

Fig. 19. Aerial imagery capturing the emergence of an englacial conduit fill at the glacier surface and development of an ice-cored esker. (a) The glacier surface is largely debris free in 2014 (WorldView-2 satellite imagery). (b) By September 2016, the former englacial conduit fill has emerged at the surface. (c–e) The continued emergence and build-up of these deposits between September 2016 and May 2019 (UAV imagery) has resulted in significant elevation increases in this area (f) and the development of a substantial ice-cored esker complex (g). The field photograph was taken in May 2019.

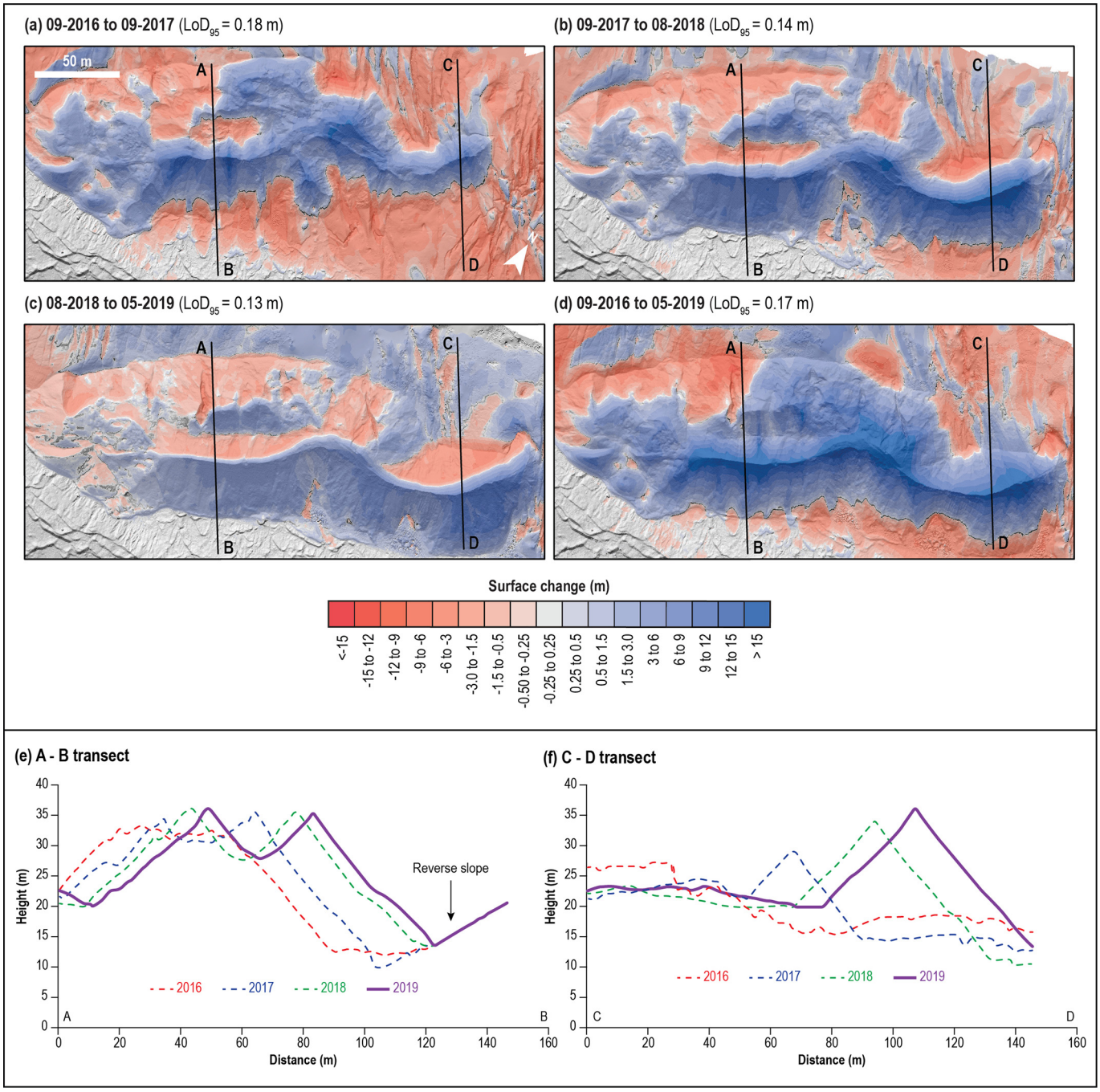

Fig. 20. (a–d) DEMs of Difference (DoDs) for the ice-cored esker at the southern margin (Area 2). Increases in elevation are indicated by blue colours, while decreases are indicated by red colours. Blank areas, where the hillshade is visible, represent areas with no detectable change. The locations of transects (shown in (e) and (f)) are indicated by the black lines annotated with letters. White polygons in (a) – (d) mask water bodies. Note, the 2019 UAV survey was conducted at the beginning of the melt season (May 2019), whereas the 2016–2018 surveys were undertaken towards the end of the melt season (August/September). For location, see Fig. 16.

repeat UAV surveying has revealed intrazonal landsystem change along much of the southern margin, characterized by a switch in the process-form regime from recessional sawtooth moraine production to the development of ice-cored terrain that includes ice-cored push moraines and a large multi-crested ice-cored esker (Section 5; Fig. 23). This ice-cored assemblage is unusual in the context of active temperate glacial landsystems as the development of ice-cored/hummocky terrain in such settings is typically precluded by limited supraglacial debris cover (cf. Evans, 2003a, 2003b). The intrazonal/azonal sediment-landform assemblages at Fjallsjökull exemplify the important role that local variations in, for example, topography and glacier surface debris cover can play in the process-form response of individual active temperate outlet glaciers.

7. Conclusions

The glacial geomorphology and surficial geology of the Fjallsjökull foreland has been mapped using a combination of LiDAR data (2011–2012), historical aerial photographs (1945–1998) and repeat UAV imagery (2016–2019). Using these remotely-sensed datasets, we have compiled two glacial landsystem maps, namely a small-scale (1: 15,000 scale) map based on the LiDAR data and aerial photographs

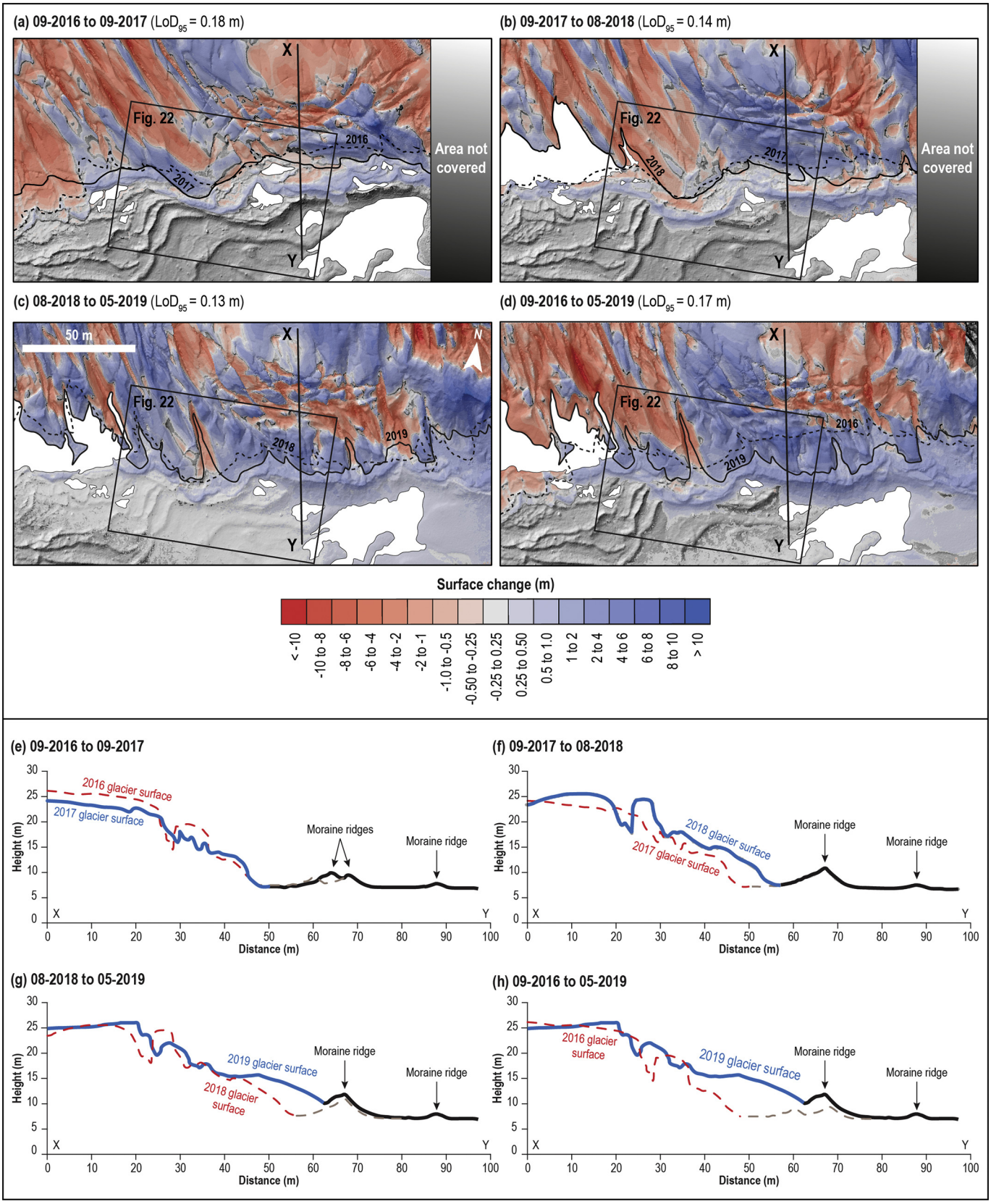

Fig. 21. DEMs of Difference (DoDs) for part of the southern glacier margin (Area 3). Increases in elevation are indicated by blue colours, while decreases are indicated by red colours. Blank areas, where the underlying hillshade is visible, represent areas with no detectable change. The dashed and solid black lines show positions of the ice margin. The lettered lines indicate the locations of transects shown in (e)–(h). Water bodies in (a)–(d) are masked by white polygons. Note, the 2019 UAV survey was conducted at the beginning of the melt season (May 2019), whereas the 2016–2018 surveys were undertaken towards the end of the melt season (August/September). For location, see Fig. 16.

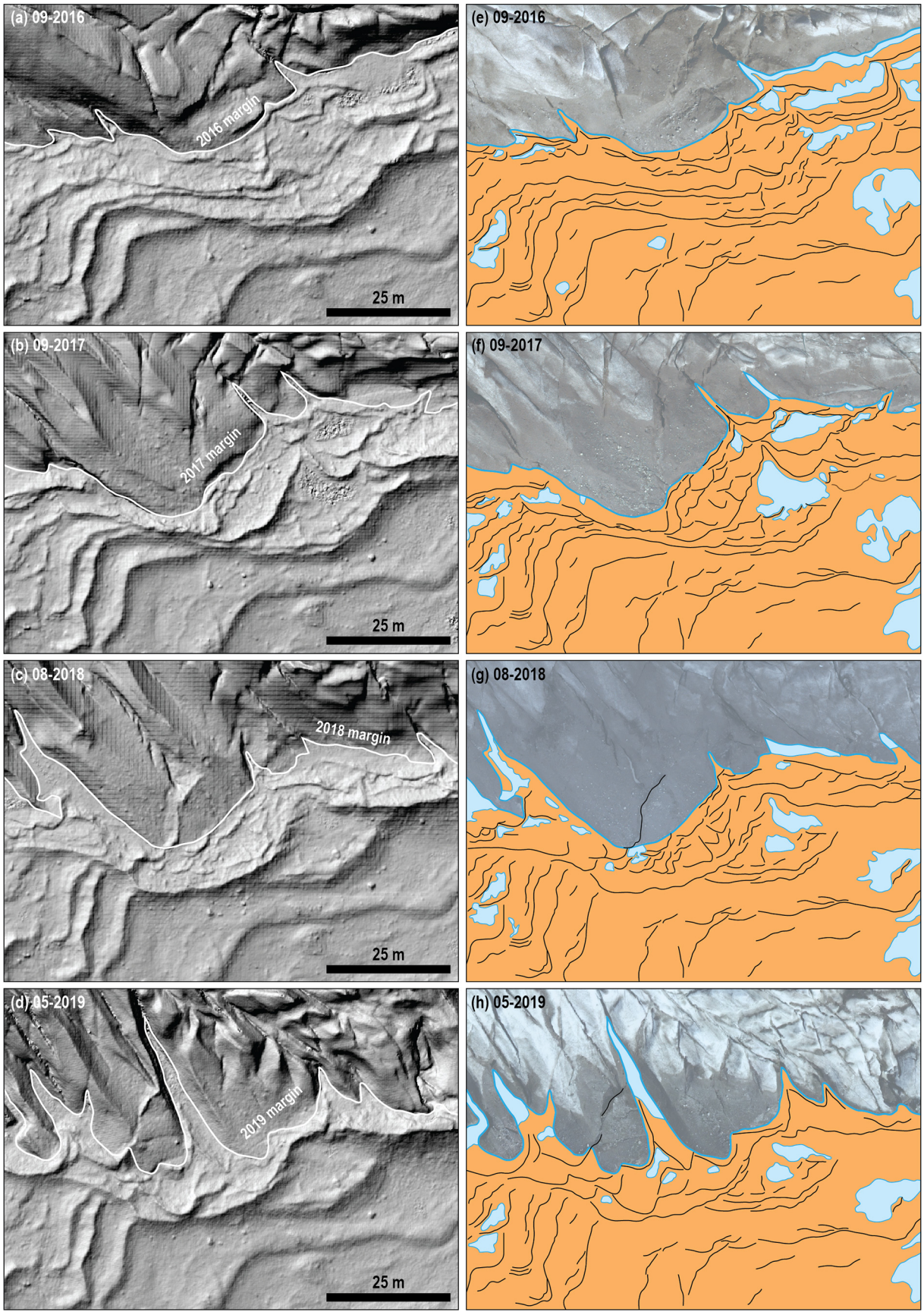

Fig. 22. UAV-derived hillshade relief models (a–d) and accompanying geomorphological map extracts (e–f) that illustrate the construction of multiple moraines (i.e. sub-annual moraines) in three consecutive years (2016–2017, 2017–2018, 2018–2019). Re-advances during this period almost entirely obliterated moraines formed in the previous year; the outermost moraine (s) are locally superimposed (b, d) or bulldozed into larger ridges (c). Note, the 2019 UAV survey was conducted at the beginning of the melt season (May 2019), whereas the 2016–2018 surveys were undertaken towards the end of the melt season (August/September). For location, see Fig. 21.

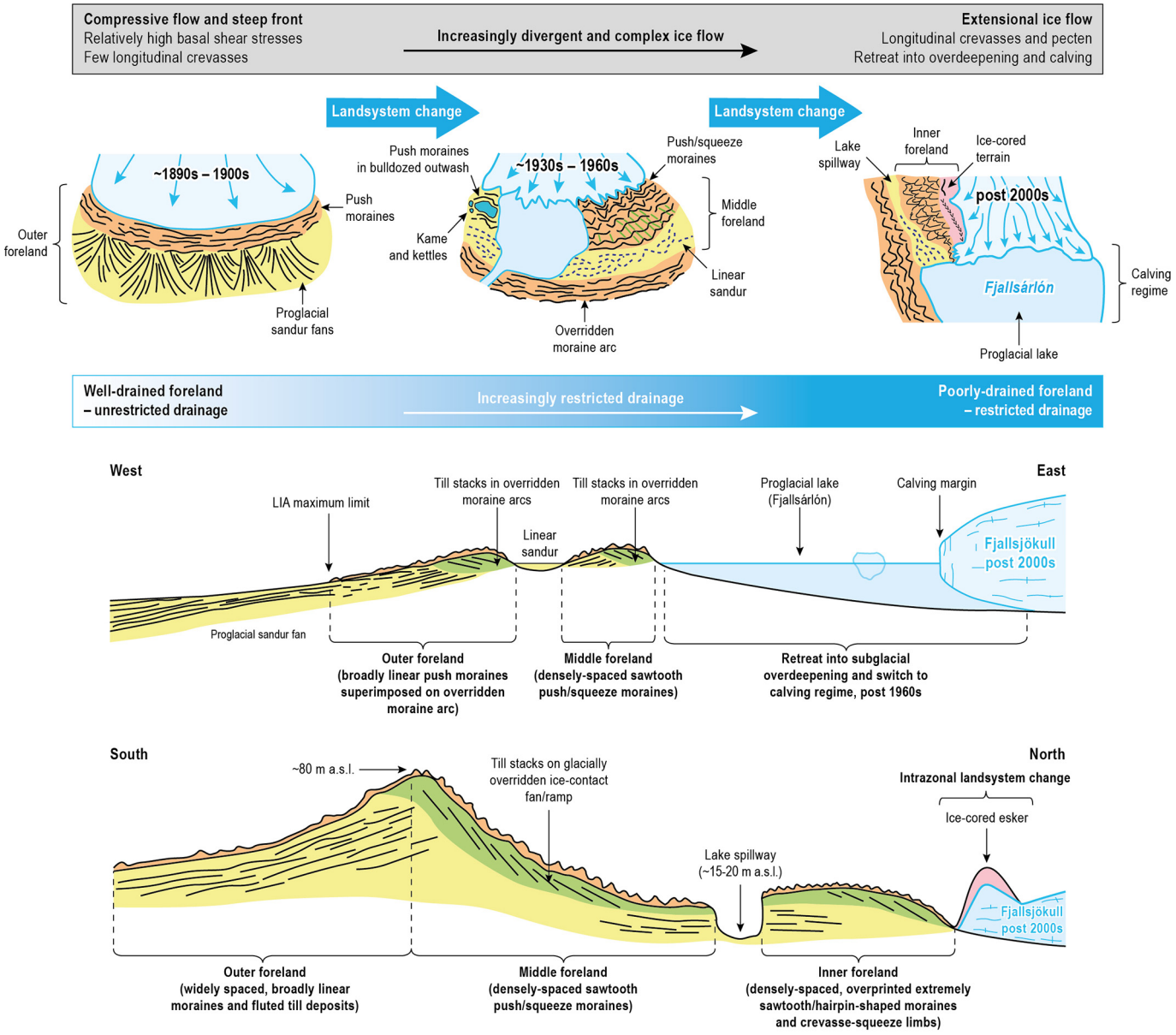

Fig. 23. Conceptual diagram (not to scale) illustrating the evolution of process-form regimes during the historical recession of Fjallsjökull. The maximum elevation (~80 m a.s.l.) of the overridden ice-contact fan/ramp is indicated, along with the elevation of the spillway floor (~15–20 m a.s.l.).

(Supplementary Material 1) and a large-scale (1: 2000 scale) map based on UAV-captured imagery from May 2019 (Supplementary Material 2). This mapping, together with the repeat UAV monitoring, has facilitated an assessment of the spatial and temporal evolution of process-form regimes at the glacier margin since the LIA maximum.

Our assessment of the Fjallsjökull glacial landsystem signature has revealed distinct landform patterns that define three landform zones across the foreland. Landform zone 1, in the outer foreland, is characterized by proglacial outwash (sandur) fans and overridden moraine arcs. Landform zone 2, in the middle foreland, contains (a) closely spaced and locally superimposed, sawtooth moraines and (b) ice margin-parallel outwash tracts. Landform zone 3, at the southern glacier margin, comprises extremely sawtooth/hairpin moraines and connected crevasse-squeeze ridge limbs, which have been constructed on a sub-annual basis since the early 2000s. This landform zonation reflects (a) a transition from unconfined proglacial drainage to progressively poorly drained and constrained conditions, and (b) the development of increasingly pronounced radial crevassing. Importantly, the key control on drainage conditions is emerging proglacial topography constructed by the glacier itself (overridden moraine arcs, glacially overridden ice-contact fans/ramps), rather than bedrock topography. Similar process-form regime changes have been identified in other glaciers in the region and thus it appears that they are a diagnostic characteristic of the active temperate glacial landsystem.

We have also identified localized (azonal/intrazonal) sediment-landform assemblages at Fjallsjökull that do not typically occur within in active temperate glacial landsystems, including fluted hummocky terrain, ice-cored/hummocky terrain, and localized kame and kettle topography. In particular, repeat UAV monitoring (2016–2019) has allowed us to capture a switch from sub-annual push/squeeze moraine formation to the development of ice-cored terrain. Our landsystem mapping and UAV monitoring at Fjallsjökull has demonstrated the important influence of local factors (e.g. topography, glacier surface debris cover) in the process-form response of individual active temperate outlet glaciers. Local variations in boundary conditions can lead to azonal/intrazonal landsystem change and localized overprinting of the diagnostic active temperate glacial landsystem signature. These findings are of high importance in a palaeoglaciological context as this indicates that

certain sediment-landform assemblages in ancient deglaciated terrain can record site-specific (e.g. topographic) controls rather than overall glaciodynamic or palaeoclimatic conditions.

Supplementary data to this article can be found online at https://doi.org/10.1016/j.geomorph.2020.107192.

Declaration of competing interest

The authors declare that they have no known competing financial interests or personal relationships that could have appeared to influence the work reported in this paper.

Acknowledgements

Fieldwork was supported by grants from the British Society for Geomorphology and the Geologists' Association, which are hereby gratefully acknowledged. Regína Hreinsdóttir and Helga Árnadóttir (both Vatnajökull National Park) are thanked for granting permission to undertake fieldwork and UAV surveying at Fjallsjökull. Research declarations were also provided by RANNÍS (The Icelandic Centre for Research) for overseas research in Iceland. We are grateful to Tómas Jóhannesson for kindly providing access to the Icelandic Meteorological Office/University of Iceland LiDAR data. We thank two anonymous reviewers for comments that helped to improve this paper.

References

Benn, D.I., 1995. Fabric signature of subglacial till deformation, Breidamerkurjokull, Iceland. Sedimentology 42, 735–747.
Benn, D.I., Evans, D.J.A., 1996. The interpretation and classification of subglacially-825 deformed materials. Quat. Sci. Rev. 15, 23–52.
Benn, D.I., Kirkbride, M.P., Owen, L.A., Brazier, V., 2003. Glaciated valley landsystems. In: Evans, D.J.A. (Ed.), Glacial Landsystems. Arnold, London, pp. 372–406.
Bennett, G.L., Evans, D.J.A., 2012. Glacier retreat and landform production on an overdeepened glacier foreland: the debris- charged glacial landsystem at Kviarjokull, Iceland. Earth Surf. Process. Landf. 37, 1584–1602.
Bennett, G.L., Evans, D.J.A., Carbonneau, P., Twigg, D.R., 2010. Evolution of a debris-charged glacier landsystem, Kviarjokull, Iceland. Journal of Maps 6, 40–76.
Björnsson, H., Pálsson, F., Sigurðsson, O., Flowers, G.E., 2003. Surges of glaciers in Iceland. Ann. Glaciol. 36, 82–90.
Boulton, G.S., 1986. Push-moraines and glacier-contact fans in marine and terrestrial environments. Sedimentology 33, 677–698.
Boulton, G.S., 1987. A theory of drumlin formation by subglacial sediment deformation. In: Menzies, J., Rose, J. (Eds.), Drumlin Symposium. Balkema, Rotterdam, pp. 25–80.
Boulton, G.S., Hindmarsh, R.C.A., 1987. Sediment deformation beneath glaciers: rheology and sedimentological consequences. Journal of Geophysical Research: Earth Surface 92, 9059–9082.
Boulton, G.S., Dobbie, K.E., Zatsepin, S., 2001. Sediment deformation beneath glaciers and its coupling to the subglacial hydraulic system. Quat. Int. 86, 3–28.
Bradwell, T., 2004. Lichenometric dating in southeast Iceland: the size-frequency approach. Geogr. Ann. 86A, 31–41.
Bradwell, T., Sigurðsson, O., Everest, J., 2013. Recent, very rapid retreat of a temperate glacier in SE Iceland. Boreas 42, 959–973.
Brasington, J., Langham, J., Rumsby, B., 2003. Methodological sensitivity of morphometric estimates of coarse fluvial sediment transport. Geomorphology 53, 299–316.
Chandler, B.M.P., Evans, D.J.A., Roberts, D.H., 2016a. Characteristics of recessional moraines at a temperate glacier in SE Iceland: insights into patterns, rates and drivers of glacier retreat. Quat. Sci. Rev. 135, 171–205.
Chandler, B.M.P., Evans, D.J.A., Roberts, D.H., 2016b. Recent retreat at a temperate Icelandic glacier in the context of the last ~80 years of climate change in the North Atlantic region. Arktos 2, article 24.
Chandler, B.M.P., Evans, D.J.A., Roberts, D.H., Ewertowski, M., Clayton, A.I., 2016c. Glacial geomorphology of the Skálafellsjökull foreland, Iceland: a case study of 'annual' moraines. Journal of Maps 12, 905–916.
Chandler, B.M.P., Lovell, H., Boston, C.M., Lukas, S., Barr, I.D., Benediktsson, Í.Ö., Benn, D.I., Clark, C.D., Darvill, C.M., Evans, D.J.A., Ewertowski, M.W., Loibl, D., Margold, M., Otto, J.-C., Roberts, D.H., Stokes, C.R., Storrar, R.D., Stroeven, A.P., 2018. Glacial geomorphological mapping: a review of approaches and frameworks for best practice. Earth Sci. Rev. 185, 806–846.
Chandler, B.M.P., Chandler, S.J.P., Evans, D.J.A., Ewertowski, M.W., Lovell, H., Roberts, D.H., Schaefer, M., Tomczyk, A.M., 2020. Sub-annual moraine formation at an active temperate glacier. Earth Surf. Process. Landf. (in press).
Cucchiaro, S., Maset, E., Fusiello, A., Cazorzi, F., 2018. 4D-SfM photogrammetry for monitoring sediment dynamics in a debris-flow catchment: software testing and results comparison. International Archives of the Photogrammetry, Remote Sensing and Spatial Information Sciences 42, 281–288.
Darvill, C.M., Stokes, C.R., Bentley, M.J., Evans, D.J.A., Lovell, H., 2017. Dynamics of former ice lobes of the southernmost Patagonian Ice Sheet based on a glacial landsystems approach. J. Quat. Sci. 32, 857–876.
Dell, R., Carr, R., Phillips, E., Russell, A.J., 2019. Response of glacier flow and structure to proglacial lake development and climate at Fjallsjökull, south-east Iceland. J. Glaciol. 65, 321–336.
Etzelmüller, B., Hagen, J., Vatne, G., Ødegård, R., Sollid, J., 1996. Glacial debris accumulation and sediment deformation influenced by permafrost: examples from Svalbard. Ann. Glaciol. 22, 53–62.
Etzelmüller, B., Farbrot, H., Guðmundsson, Á., Humlum, O., Tveito, O.E., Björnsson, H., 2007. The regional distribution of mountain permafrost in Iceland. Permafr. Periglac. Process. 18 (2), 185–199.
Evans, D.J.A., 2000. A gravel outwash/deformation till continuum, Skalafellsjokull, Iceland. Geogr. Ann. 82A, 499–512.
Evans, D.J.A. (Ed.), 2003a. Glacial Landsystems. Arnold, London (532 pp).
Evans, D.J.A., 2003b. Ice-marginal terrestrial landsystems: active temperate glacier margins. In: Evans, D.J.A. (Ed.), Glacial Landsystems. Arnold, London, pp. 12–43.
Evans, D.J.A., 2005. The glacier-marginal landsystems of Iceland. In: Caseldine, C., Russell, A., Harðardóttir, J., Knudsen, Ó. (Eds.), Iceland – Modern Processes and Past Environments. Developments in Quaternary Sciences 5, pp. 93–126.
Evans, D.J.A., 2009. Glacial geomorphology at Glasgow. Scott. Geogr. J. 125, 285–320.
Evans, D.J.A., 2013. The glacial and periglacial research – geomorphology and retreating glaciers. In: Shroder, J., Giardino, R., Harbor, J. (Eds.), Treatise on Geomorphology. Glacial and Periglacial Geomorphology 8. Academic Press, San Diego, CA, pp. 460–478.
Evans, D.J.A., 2018. Till: A Glacial Process Sedimentology. The Cryosphere Science Series, Wiley Blackwell, Chichester.
Evans, D.J.A., Benn, D.I. (Eds.), 2004. A Practical Guide to the Study of Glacial Sediments. Arnold, London.
Evans, D.J.A., Chandler, B.M.P., 2018. Geology, physiography and glaciology of SE Iceland. In: Evans, D.J.A. (Ed.), Glacial Landsystems of Southeast Iceland – Quaternary Applications: Field Guide. Quaternary Research Association, London, pp. 1–19.
Evans, D.J.A., Ewertowski, M.W., 2018. The glacial landsystem of the Fláajökull north lobe. In: Evans, D.J.A. (Ed.), Glacial Landsystems of Southeast Iceland – Quaternary Applications: Field Guide. Quaternary Research Association, London, pp. 243–258.
Evans, D.J.A., Hiemstra, J.F., 2005. Till deposition by glacier submarginal, incremental thickening. Earth Surf. Process. Landf. 30, 1633–1662.
Evans, D.J.A., Orton, C., 2015. Heinabergsjökull and Skalafellsjökull, Iceland: active temperate piedmont lobe and outwash head glacial landsystem. Journal of Maps 11, 415–431.
Evans, D.J.A., Twigg, D.R., 2002. The active temperate glacial landsystem: a model based on Breiðamerkurjökull and Fjallsjökull, Iceland. Quat. Sci. Rev. 21, 2143–2177.
Evans, D.J.A., Lemmen, D.S., Rea, B.R., 1999. Glacial landsystems of the southwest Laurentide Ice Sheet: modern Icelandic analogues. J. Quat. Sci. 14, 673–691.
Evans, D.J.A., Phillips, E.R., Hiemstra, J.F., Auton, C.A., 2006. Subglacial till: formation, sedimentary characteristics and classification. Earth Sci. Rev. 78, 115–176.
Evans, D.J.A., Shand, M., Petrie, G., 2009. Maps of the snout and proglacial landforms of Fjallsjökull, Iceland (1945, 1965, 1998). Scott. Geogr. J. 125, 304–312.
Evans, D.J.A., Nelson, C.D., Webb, C., 2010. An assessment of fluting and till esker formation on the foreland of Sandfellsjökull, Iceland. Geomorphology 114, 453–465.
Evans, D.J.A., Young, N.J.P., Cofaigh, C.Ó., 2014. Glacial geomorphology of terrestrial-terminating fast flow lobes/ice stream margins in the southwest Laurentide Ice Sheet. Geomorphology 204, 86–113.
Evans, D.J.A., Ewertowski, M., Orton, C., 2016a. Fláajökull (north lobe), Iceland: active temperate piedmont lobe glacial landsystem. Journal of Maps 12, 777–789.
Evans, D.J.A., Roberts, D.H., Evans, S.C., 2016b. Multiple subglacial till deposition: a modern exemplar for Quaternary palaeoglaciology. Quat. Sci. Rev. 145, 183–203.
Evans, D.J.A., Ewertowski, M., Orton, C., 2017a. Skaftafellsjökull, Iceland: glacial geomorphology recording glacier recession since the Little Ice Age. Journal of Maps 13, 358–368.
Evans, D.J.A., Ewertowski, M., Orton, C., 2017b. The glaciated valley landsystem of Morsárjökull, southeast Iceland. Journal of Maps 13, 909–920.
Evans, D.J.A., Roberts, D.H., Hiemstra, J.F., Nye, K.M., Wright, H., Steer, A., 2018a. Submarginal debris transport and till formation in active temperate glacier systems: the southeast Iceland type locality. Quat. Sci. Rev. 195, 72–108.
Evans, D.J.A., Ewertowski, M., Orton, C., Graham, D.J., 2018b. The glacial geomorphology of the ice cap piedmont lobe landsystem of East Myrdalsjokull, Iceland. Geosciences 8, 194.
Evans, D.J.A., Ewertowski, M., Roberts, D.H., 2018c. Glacial landsystem development at Fjallsjökull. In: Evans, D.J.A. (Ed.), Glacial Landsystems of Southeast Iceland: Quaternary Applications – Field Guide. Quaternary Research Association, London, pp. 224–241.
Evans, D.J.A., Ewertowski, M.W., Orton, C., 2019a. The glacial landsystem of Hoffellsjökull, SE Iceland: contrasting geomorphological signatures of active temperate glacier recession driven by ice lobe and bed morphology. Geogr. Ann. 101A, 225–248.
Evans, D.J.A., Guðmundsson, S., Vautrey, J.L., Fearnyough, K., Southworth, W.G., 2019b. Testing lichenometric techniques in the production of a new growth-rate (curve) for the Breiðamerkurjökull foreland, Iceland, and the analysis of potential climatic drivers of glacier recession. Geogr. Ann. 101A, 225–248.
Evans, D.J.A., Atkinson, N., Phillips, E., 2020. Glacial geomorphology of the Neutral Hills Uplands, southeast Alberta, Canada: the process-form imprints of dynamic ice streams and surging ice lobes. Geomorphology 350, 106910.
Evans, D.J.A., Ewertowski, M.W., Tomczyk, A.M., Chandler, B.M.P. In prep. The Spatial and Temporal Evolution of a Glacial Landsystem Signature at an Outwash Head/Depositional Overdeepening, Hrútárjökull–Fjallsjökull, Iceland.
Everest, J., Bradwell, T., Jones, L.D., Hughes, L., 2017. The geomorphology of Svínafellsjökull and Virkisjökull-Falljökull glacier forelands, southeast Iceland. Journal of Maps 13, 936–945.

Ewertowski, M.W., Evans, D.J.A., Roberts, D.H., Tomczyk, A.M., Ewertowski, W., Pleksot, K., 2019a. Quantification of historical landscape change on the foreland of a receding polythermal glacier, Hørbyebreen, Svalbard. Geomorphology 325, 40–54.
Ewertowski, M.W., Tomczyk, A.M., Evans, D.J.A., Roberts, D.H., Ewertowski, W., 2019b. Operational framework for rapid, very-high resolution mapping of glacial geomorphology using low-cost unmanned aerial vehicles and structure-from-motion approach. Remote Sens. 11, 65.
Eyþórsson, J., 1935. On the variations of glaciers in Iceland. Some studies made in 1931. Geogr. Ann. 17, 121–137.
Eyþórsson, J., 1963. Variation of Iceland glaciers 1931–1960. Jökull 13, 31–33.
Griffiths, J.S., Martin, C.J. (Eds.), 2017. Engineering Geology and Geomorphology of Glaciated and Periglaciated Terrains: Engineering Group Working Party Report. Engineering Geology Special Publication 28. The Geological Society, London (953 pp).
Guðmundsson, M.T., 2000. Mass balance and precipitation on the summit plateau of Öræfajökull, SE Iceland. Jökull 48, 49–54.
Hannesdóttir, H., Björnsson, H., Pálsson, F., Aðalgeirsdóttir, G., Guðmundsson, S., 2014. Variations of southeast Vatnajökull ice cap (Iceland) 1650–1900 and reconstruction of the glacier surface geometry at the Little Ice Age maximum. Geogr. Ann. 97A, 237–264.
Hannesdóttir, H., Björnsson, H., Pálsson, F., Aðalgeirsdóttir, G., Guðmundsson, S., 2015. Area, volume and mass changes of southeast Vatnajökull ice cap, Iceland, from the Little Ice Age maximum in the late 19th century to 2010. Cryosphere 9, 565–585.
Hart, J.K., Rose, K.C., Clayton, A., Martinez, K., 2015. Englacial and subglacial water flow at Skálafellsjökull, Iceland derived from ground penetrating radar, in situ Glacsweb probe and borehole water level measurements. Earth Surf. Process. Landf. 40, 2071–2083.
Martinez, K., Hart, J.K., Basford, P.J., Clayton, A.I., Bragg, G.M., Ward, T., Young, D.S., 2019a. Surface melt-driven seasonal behaviour (englacial and subglacial) from a soft-bedded temperate glacier recorded by in situ wireless probes. Earth Surf. Process. Landf. 44, 1769–1782.
Hart, J.K., Martinez, K., Basford, P.J., Clayton, A.I., Robson, B.A., Young, D.S., 2019b. Surface melt driven summer diurnal and winter multi-day stick-slip motion and till sedimentology. Nat. Commun. 10, 1599.
Howarth, P.J., Welch, R., 1969a. Breiðamerkurjökull, South-east Iceland, August 1945. 1: 30,000 scale map. University of, Glasgow.
Howarth, P.J., Welch, R., 1969b. Breiðamerkurjökull, South-east Iceland, August 1965. 1: 30,000 scale map. University of, Glasgow.
Ingólfsson, Ó, Benediktsson, Í.Ö., Schomacker, A., Kjær, K.H., Brynjólfsson, S., Jónsson, S.A., Korsgaard, N.J., Johnson, M.J., 2016. Glacial geological studies of surge-type glaciers in Iceland — Research status and future challenges. Earth-Science Reviews 152, 37–69.
James, M.R., Robson, S., Smith, M.W., 2017. 3-D uncertainty-based topographic change detection with structure-from-motion photogrammetry: precision maps for ground control and directly georeferenced surveys. Earth Surf. Process. Landf. 42, 1769–1788.
Jóhannesson, T., Björnsson, H., Magnússon, E., Guðmundsson, S., Pálsson, F., Sigurðsson, O., Thorsteinsson, T., Berthier, E., 2013. Ice-volume changes, bias estimation of mass-balance measurements and changes in subglacial lakes derived by lidar mapping of the surface of Icelandic glaciers. Ann. Glaciol. 54, 63–74.
Jónsson, S.A., Schomacker, A., Benediktsson, Í.Ö., Ingólfsson, Ó., Johnson, M.D., 2014. The drumlin field and the geomorphology of the Múlajökull surge-type glacier, central Iceland. Geomorphology 207, 213–220.
Kirkbride, M.P., 2000. Ice marginal geomorphology and Holocene expansion of debris-covered Tasman Glacier, New Zealand. In: Nakawo, M., Raymond, C., Fountain, A. (Eds.), Debris-Covered Glaciers. IAHS Publication 264, Wallingford, pp. 211–217.
Kjær, K.H., Krüger, J., 2001. The final phase of dead-ice moraine development: processes and sediment architecture, Kotlujokull, Iceland. Sedimentology 48, 935–952.
Krüger, J., 1994. Glacial processes, sediments, landforms, and stratigraphy in the terminus region of Mýrdalsjökull, Iceland. Folia Geogr. Dan. 21, 1–233.
Krüger, J., 1995. Origin, chronology and climatological significance of annual-moraine ridges at Myrdalsjökull, Iceland. The Holocene 5, 420–427.
Krüger, J., 1996. Moraine ridges formed from subglacial frozen-on sediment slabs and their differentiation from push moraines. Boreas 25, 57–64.
Krüger, J., Kjær, K.H., 2000. De-icing progression of ice-cored moraines in a humid, subpolar climate, Kötlujökull. Iceland. Holocene. 10, 737–747.
Lukas, S., Nicholson, L.I., Ross, F.H., Humlum, O., 2005. Formation, meltout processes and landscape alteration of High-Arctic ice-cored moraines—examples from Nordenskiöld Land, Central Spitsbergen. Polar Geogr. 29, 157–187.
Lukas, S., Benn, D.I., Boston, C.M., Brook, M., Coray, S., Evans, D.J.A., Graf, A., Kellerer-Pirklbauer, A., Kirkbride, M.P., Krabbendam, M., Lovell, H., Machiedo, M., Mills, S.C., Nye, K., Reinardy, B.T.I., Ross, F.H., Signer, M., 2013. Clast shape analysis and clast transport paths in glacial environments: a critical review of methods and the role of lithology. Earth Sci. Rev. 121, 96–116.
Magnússon, E., Pálsson, F., Björnsson, H., Guðmundsson, S., 2012. Removing the ice cap of Öraefajokull central volcano, SE Iceland: Mapping and interpretation of bedrock topography, ice volumes, subglacial troughs and implications for hazards assessments. Jökull 62, 131–150.
Maizels, J.K., 1993. Lithofacies variations within sandur deposits: the role of runoff regime, flow dynamics and sediment supply characteristics. Sediment. Geol. 85, 299–325.
Marren, P.M., 2002. Glacier margin fluctuations, Skaftafellsjökull, Iceland: Implications for Sandur evolution. Boreas 31, 75–81.
Marren, P.M., 2005. Magnitude and frequency in proglacial rivers: a geomorphological and sedimentological perspective. Earth Sci. Rev. 70, 203–251.
Midgley, N.G., Tonkin, T.N., Graham, D.J., Cook, S.J., 2018. Evolution of high-Arctic glacial landforms during deglaciation. Geomorphology 311, 63–75.
Phillips, E.R., Finlayson, A., Bradwell, T., Everest, J., Jones, L., 2014. Structural evolution triggers a dynamic reduction in active glacier length during rapid retreat: evidence from Falljökull, SE Iceland. Journal of Geophysical Research: Earth Surface 119, 2194–2208.
Price, R.J., 1969. Moraines, sandar, kames and eskers near Breiðamerkurjökull, Iceland. Trans. Inst. Br. Geogr. 46, 17–43.
Price, R.J., 1970. Moraines at Fjallsjökull, Iceland. Arct. Alp. Res. 2, 27–42.
Price, R.J., 1982. Changes in the proglacial area of Breiðamerkurjökull, southeastern Iceland: 1890–1980. Jökull 32, 29–35.
Price, R.J., Howarth, P.J., 1970. The evolution of the drainage system (1904–1965) in front of Breiðamerkurjökull, Iceland. Jökull 20, 27–37.
Roberts, D.H., 1995. The Development of Criteria to Distinguish Glaciotectonic and Glaciomarine Sedimentary Environments. Unpublished PhD thesis. University of Southampton.
Rose, J., Whiteman, C.A., Lee, J., Branch, N.P., Harkness, D.D., Walden, J., 1997. Mid- and late-Holocene vegetation, surface weathering and glaciation, Fjallsjökull, southeast Iceland. The Holocene 7, 457–471.
Russell, A.J., Knight, P.G., van Dijk, T.A.G.P., 2001. Glacier surging as a control on the development of proglacial, fluvial landforms and deposits, Skeiðarársandur, Iceland. Global Planetary Change 28, 163–174.
Schaefer, M., Teeuw, R., Day, S., Zekkos, D., Weber, P., Meredith, T., Van Westen, C.J., 2020. Low-cost UAV surveys of hurricane damage in Dominica: automated processing with co-registration of pre-hurricane imagery for change analysis. Nat. Hazards (in press).
Schomacker, A., Kjær, K.H., 2007. Origin and de-icing of multiple generations of ice-cored moraines at Brúarjökull, Iceland. Boreas 36, 411–425.
Schomacker, A., Kjær, K.H., 2008. Quantification of dead-ice melting in ice-cored moraines at the high-Arctic glacier Holmströmbreen, Svalbard. Boreas 37, 211–225.
Schomacker, A., Benediktsson, Í.Ö., Ingólfsson, Ó., 2014. The Eyjabakkajökull glacial landsystem, Iceland: geomorphic impact of multiple surges. Geomorphology 218, 98–107.
Sharp, M.J., 1984. Annual moraine ridges at Skálafellsjökull, southeast Iceland. J. Glaciol. 30, 82–93.
Sigurðsson, O., Williams, R.S., 2008. Geographic names of Icelandic glaciers: historic and modern. US Geological Survey Professional Paper 1746 (225 pp).
Sigurðsson, O., Jónsson, T., Jóhannesson, T., 2007. Relation between glacier-termini variations and summer temperature in Iceland since 1930. Ann. Glaciol. 46, 170–176.
Sutherland, J.L., Carrivick, J.L., Evans, D.J.A., Shulmeister, J., Quincey, D.J., 2019. The Tekapo Glacier, New Zealand, during the Last Glacial Maximum: an active temperate glacier influenced by intermittent surge activity. Geomorphology 343, 183–210.
Thórarinsson, S., 1943. Vatnajökull: scientific results of the Swedish–Icelandic investigations 1936–37–38. Chapter XI. Oscillations of the Icelandic glaciers in the last 250 years. Geogr. Ann. 25, 1–54.
Tonkin, T.N., Midgley, N.G., Cook, S.J., Graham, D.J., 2016. Ice-cored moraine degradation mapped and quantified using an unmanned aerial vehicle: a case study from a polythermal glacier in Svalbard. Geomorphology 258, 1–10.
Waller, R.I., van Dijk, T.A.G.P., Knudsen, Ó., 2008. Subglacial bedforms and conditions associated with the 1991 surge of Skeiðarárjökull, Iceland. Boreas 37, 179–194.
Waller, R.I., Evans, D.J.A., Hiemstra, J.F., 2018. Glacial landsystem development at Skeiðarárjökull. In: Evans, D.J.A. (Ed.), Glacial Landsystems of Southeast Iceland – Quaternary Applications: Field Guide. Quaternary Research Association, London, pp. 86–101.
Wheaton, J.M., Brasington, J., Darby, S.E., Merz, J., Pasternack, G.B., Sear, D., Vericat, D., 2010. Linking geomorphic changes to salmonid habitat at a scale relevant to fish. River Res. Appl. 26, 469–486.